# Characterization Of A Microfluidic Bubble Removal System Using A Converging-Diverging Nozzle

BY

Carlos Ng Pitti
B.S., University of Illinois at Chicago, Chicago, 2012

THESIS

Submitted as partial fulfillment of the requirements
for the degree of Master of Science in Bioengineering
in the Graduate College of the
University of Illinois at Chicago, 2016

Chicago, Illinois

Defense Committee:
David Eddington, Chair and Advisor
Jun Cheng
Thomas Royston

*This thesis is dedicated to Lide and Horacio.*

ACKNOWLEDGEMENTS

I would like to thank my family for helping me through my career and for their unconditional support. Also, thank you Dr. Eddington for giving me the opportunity to work in your laboratory, being my research advisor and supporting me financially. Finally, I want to thanks my thesis committee, professors, collaborators and lab members that I met. It was a pleasure to work with all of you.

TABLE OF CONTENTS

LIST OF FIGURES

FIGURE PAGE

# LIST OF ABBREVIATIONS

| | |
|---|---|
| CCD | Charged Couple Device |
| °C | Degrees Celsius |
| DI | Deionized |
| DMSO | Dimethyl Sulfoxide |
| FITC | Fluorescein Isothiocyanate |
| IPA | Isopropyl Alcohol |
| ID | Inner Diameter |
| L | Liter |
| MEMS | Microelectromechanical Systems |
| µm | Micrometer |
| µL | Microliter |
| mm | Millimeter |
| $N_2$ | Nitrogen |
| OD | Outer Diameter |
| pL | Picoliter |
| PCR | Polymerase Chain Reaction |
| PDMS | Polydimethylsiloxane |
| PTFE | Poly (tetrafluoro ethylene) |
| RPM | Revolutions per Minute |

LIST OF ABBREVIATIONS (continued)

| | |
|---|---|
| sccm | Standard Cubic Centimeters per Minute |
| Si | Silicon |
| s | Seconds |
| UV | Ultraviolet |

## SUMMARY

Undesired bubble formation has been a major problem in microfluidics devices. Depending on the application, air bubbles can affect the performance of microfluidic devices and lead to failure. Recent microfabrication techniques have originated several methods, such as bubble traps and debubblers, to solve this problem. However, these methods require large vacuum pumps or air compressors to remove the air bubbles. In this project, a microfluidic vacuum source generator is used and characterized in order to remove air bubbles in a non-invasive way. This miniaturized vacuum source is based on a converging-diverging nozzle device which is able to generate a range of negative pressures, depending on the input flow of a pressurized gas tank. In order to quantify and characterize its bubble removal rate, its performance was tested using a double layer PDMS device. In addition, the bubble removal system was applied on devices that contain partially filled channels. Finally, future improvements to this bubble removal system are discussed as well as the benefits of this system compared to other approaches.

# CHAPTER 1: INTRODUCTION AND BACKGROUND

## 1.1 Microfluidics

Microfluidic technology has been around for the last 40 years, not only by miniaturizing existing systems but also innovating different biological fields. Microfluidics is defined as the science and technology that manipulates any type of fluid at the micro scale, from attoliters ($10^{-18}$ L) to microliters ($10^{-6}$ L) (Whitesides, 2006a). There are multiple reasons for its success, such as the handling of small fluid samples, portability, reliability, safety, high repeatability, lower power consumption, fast system response, less sources of error and user-friendly devices (Panigrahi, 2015a). In addition, the handling of microscale fluid samples leads to a reduction in size of devices which brings another set of benefits like less fabrication materials, fewer chemical reagents be consumed and reduction of waste products. However, the main reason for its success is that fluids at the microscale behave differently from conventional macroscale quantities which can be useful in many applications (Nguyen and Wereley, 2006a). These differences can be explained by the ratio of inertia to viscous forces, also known as the Reynolds number which is a dimensionless parameter that can be calculated by equation 1. At the macroscale, inertial forces are more important than viscosity which is the opposite effect at the microscale. This is important because The Reynolds numbers shows the fluid behavior.

$$\mathrm{Re} = \frac{\rho \mathrm{v} \mathrm{L}}{\mu} \qquad \text{Eq. 1}$$

Where $\rho$ is the density of the fluid (kg/m$^3$), $L$ is the cross-sectional dimension (m), $v$ is the velocity of the fluid (m/s) and $\mu$ is the viscosity of the fluid (kg/(m·s)). In a microfluidic channel, any fluid with a Reynolds number lower than 1500 indicates a laminar flow, and

a turbulent flow is indicated with a higher number than 1500 (Nguyen and Wereley, 2006b). The difference between these two types of flow is that when fluids tend to flow in a laminar manner, its behavior is more predictable compared to fluids flowing in a turbulent manner which is chaotic and unpredictable. For that reason, the field of microfluidics has evolved and expanded its applications in a vast variety of fields. For example, in laminar flow, the mixing mechanism is done by diffusion at the liquid-liquid interphase between two streams perpendicular to the flowing direction. This has been advantageous because it is a membraneless system used with a controlled diffusion for designing fuel cells (Choban et al., 2004), whole blood diagnostics (Weigl et al., 1999), pH gradients for isoelectric focusing (Macounová et al., 2000) and DNA analysis (Burns et al., 1998). However, in occasions, turbulent flow is needed to enhance mixing of fluids. This can be done by implementing serpentine channels (Liu et al., 2000), or grooves at the bottom on the channel to facilitate the contact between the two fluids leading to a complete mixture (Stroock et al., 2002).

In order to induce these two types of flows in microdevices, it is required specialized fabrication techniques that allow us to make microscale structures for the handling of small fluid quantities. Not only can these microdevices handle microscale fluids, but they also provide a high heat and mass transfer rates through a high surface-to-volume ratio (Panigrahi, 2015b). A common microfabrication procedure known as photolithography has been used to manufacture microelectromechanical systems (MEMS) devices which main advantage is to fabricate precise and accurate structures.

### 1.1.1 Photolithography

Photolithography is one of the most relevant fabrication techniques in microfluidics (Nguyen and Wereley, 2006c). It is able to achieve features sized on the micro scale range. This fabrication technique utilizes photoresists which are photosensitive epoxy that can transfer a specific design from a photomask to a substrate. The photomask can be either a chromium plate or a transparency film which will contain the desired pattern. For our purposes, the goal of the photolithography process is to cast a mold that will be used for the soft lithography process. The photolithography process starts by spinning a layer of either a positive or negative photoresists on a dehydrated silicon wafer. Positive photoresist will harden the unexposed features and negative photoresist will harden the exposed features. For this project, we used a negative photoresist called SU-8 which has three main components: the epoxy resin, a solvent and a photoinitiator. The spin speed and the viscosity of the resists will determine the height of the mold. Therefore, it is really important to choose the SU-8 with the right viscosity and use the proper spin speed to achieve the desired height. After spin coating, the wafer with the SU-8 goes through the soft bake which removes all the solvents from the photoresist. This is a crucial step because oversoft-baking will degrade the photoinitiator compound and undersoft-baking will not remove all the solvent which will prevent light to reach the photoinitiator. After that, the SU-8 layer is exposed to UV light or near UV wavelengths through the photomask. Since SU-8 is a negative photoresist, the UV light polymerized all the exposed epoxy areas. Then, the wafer goes through the post-exposure bake which improves adhesion and dry etch resistance, followed by the development step where the wafer is soaked with SU-8 developer to remove any unpolymerized areas that were not exposed to UV light.

Finally, the mold is rinsed with isopropyl alcohol (IPA) and dried using an air gun. An additional step after the photolithography process is known as silanization where the mold is placed on a desiccator with 20 µL of tridecafluoro-1,1,2,3-tetrahydrooctyl-1-trichlorosilane for a period of at least two hours to enhance the soft elastomer removal during the soft lithography process (Anderson et al., 2000). Using this microfabrication process, most microfluidic channels are between 30-300 µm (Panigrahi, 2015c). Other techniques or specialized machinery are required to achieve better resolutions such as different types of lithography, or specialized fabrication systems like the µPG 101 which is a maskless lithography system. This shows that to obtain smaller features can be challenging as well as expensive. The reason for that is because the wavelength limits the resolution of photolithography (Nguyen and Wereley, 2006d). Photolithography became an important tool for microfabrication and demonstrated its potential in different biological disciplines. For that reason, soft lithography was created to make photolithography suitable with the different biological fields.

### 1.1.2 Soft lithography

Although photolithography has been a commonly used process for the fabrication of glass and silicone microfluidic devices, it has several disadvantages such as requiring expensive equipment, complex process, not useful for protein and cells, extensive time length to go from a design to a prototype and the high toxicity of the reagents (Whitesides et al., 2001a). To overcome those problems, polymers were developed and tested as a new material. Polymers have a variety of different mechanical and chemical properties that can be used for the fabrication of microdevices (Ng et al., 2002a). Not only are polymers cheaper than glass or silicone, but they are also simple to handle. Polymers

used for microfluidics devices are polyethyleneterephthalate glycol (Barker et al., 2000), polycarbonate (Johnson et al., 2002; Olsen et al., 2002), polymethyl methacrylate (Wang et al., 2002), polystyrene (Locascio et al., 1999), polyvinylchloride and polyethylene (Becker and Locascio, 2002). However, a special type of soft polymer known as elastomer is used because of its extra set of advantages such as flexibility, ease to use and low toxicity. In addition, a new fabrication technique called soft lithography was developed from photolithography and it consists of replicating the structure from a mold in an elastomer (Ng et al., 2002b). This allows compatibility between the microfluidic device and the different biological applications. Additionally, soft lithography is a simple inexpensive process and the reagents used are not toxic compared to photolithography. The process of soft lithography starts when a mixture of an elastomer with a unpolymerized form with curing agent is prepared using a mixing ratio. Then, the mixture is poured over a mold and degassed in a desiccator. After that, the wafer is baked at 85ºC for 1 hour and 30 minutes. During this time, the elastomer polymerizes and the whole mixture solidifies resulting in a cross-linked elastomer. Once it is cured, the layer is removed from the mold and it is ready for the device assembly. After the bake, the mold can be reused to make multiple devices.

### 1.1.3 PDMS

In microfluidics, the majority of devices used for biological applications are made from a soft elastomer called polydimethylsiloxane (PDMS), which is a synthesized silicon-based organic polymer that consists of repeating $[SiO(Ch_3)_2]$ monomer units (Colas, 2005). PDMS is an outstanding material for the fabrication of microfluidics devices for several reasons, such as precise replica molding, optically transparency, low

autofluorescence and low cost (Xia and Whitesides 1998). In addition, it has low toxicity and high permeability to certain gases such as carbon dioxide and oxygen (Whitesides, 2006b). It has desirable mechanical properties such as flexibility, with a shear elastic modulus of around 250 GPa. In addition, it has a high dielectric strength (Lötters et al., 1997), and usage over a wide temperature range (Krevelen and Nijenhuis, 2009) which makes PDMS an ideal material for a variety of applications. PDMS and the curing agent are sold as a kit which is commercially available at a reasonable price. The commercially available PDMS kit includes the silicone base and the curing agent. Both components have vinyl-terminated siloxane oligomers, but the curing agent has the crosslinking siloxane oligomers such as dimethyl methylhydrogen siloxane. The base also has a platinum-based catalyst which cures the elastomer through an organometallic crosslinking reaction (Campbell et al., 1999). These two components are mixed usually in a 10:1 ratio, depending on the desired rigidity, and then baked at 85°C for 1 hour and 30 minutes. During the bake, the chains are polymerized and the whole mixture solidifies which leads to a cross-linked elastomer. PDMS can be bound to another PDMS slide or substrate by spontaneous dehydration caused by plasma treatment (Whitesides et al., 2001b).

For this project, the main PDMS properties used are its transparency and gas permeability for the functionality of the converging-diverging nozzle as a bubble removal device.

### 1.2 Bubble Formation

Bubble formation has been studied extensively in microfluidics. Undesired air bubbles have been shown to cause problems as well as been useful for different

applications. In one hand, bubbles have been useful as a driving force for a micro-rotor (Kao et al., 2007), enhancing heat and mass transfer (Kreutzer et al., 2005; Betz and Attinger, 2010) , enhancing mixing of liquids (Garstecki et al., 2006; Günther et al., 2005), enhancing stimulus and cell lysis (El-Ali et al., 2005) providing a platform for cellular biosynthesis (Choi and Montemagno, 2006) and becoming an optical switch (Jackel et al., 1990). On the other hand, bubble formation in a microfluidic device can be contributed to the channel design as seen in figure 1(B & C), temperature change (Wang et al. 2012a; Lochovsky et al., 2012a), hydrophobic materials (Monahan et al., 2001a), the complexity of the microfluidic device with gas-liquid interphases (Zhu, 2009; Lochovsky et al., 2012b) and the connection between the devices and the tubing (Skelley and Voldman, 2008a; Zheng et al., 2010a; Wang et al., 2012b). Although these are the main reasons, bubble formation is a constant problem in general microfluidic applications.

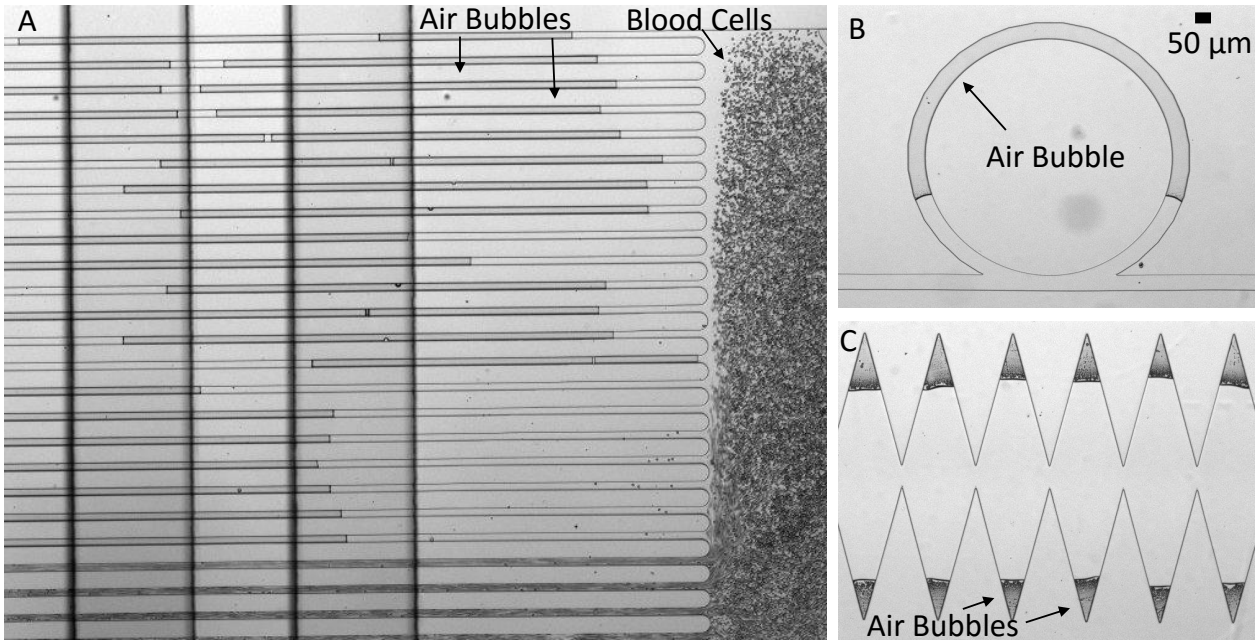


Figure 1. Schematic of microfluidic channels with trapped air bubbles. (A) Bubbles preventing the flow of blood cells. (B) Bubble trapped in a loop shape channel. (C) Bubble formation in triangular structures.

There are many applications such as single cell assays, vascular network models and cell culture in microfluidic devices that have reported experiencing problems with air bubbles. For example, a network model was unable to flow blood cells because of air bubbles were trapped in the channel (figure 1A), long-term islet culture tends to accumulate air bubbles over time (Wang et al., 2012c), a device used to study sickle cells is degassed at least 15 minutes before loading it with working sample to avoid air bubble trapping (Du et al., 2015), another device that studies vasocclusion also mentioned using the high pressure of water to remove the air bubbles (Higgins et al., 2007), a device used to study individual cells for long periods of time reported bubble formation, even though the channel design was improved to prevent them from forming (Denoual et al., 2003). The reason to avoid bubbles in microfluidics channels is because bubbles tend to grow due to the pressure difference between the outside and inside of the fluidic channel (Kang et al., 2008a) and they are hard to remove. Unwanted air bubbles can have devastating effects such as disturbing stable laminar flow (Kang et al., 2008b), inaccurate sample volumes (van Lintel et al., 2012a), channel clogging (Jensen et al., 2004; van Lintel et al., 2012b) and being cytotoxic to cells since bubbles within microfluidic channels can lead to high surface tension of the air-liquid interface and rupture the cellular membrane (Eddington, 2006a). A conventional method to remove bubbles is degassing the microfluidic device on a desiccator for a period of time. However, this method requires that you place the microfluidic device in a vacuum chamber and the process can take several minutes depending on the channel design. As a result, different strategies have been applied in order to solve this problem.

### 1.3 Current Bubble Removal Systems

There have been different mechanisms for bubble removal which are mainly, divided into two approaches: bubble traps (passive trapping) and microfluidic debubblers (active trapping). Bubble traps are integrated structures in the microfluidic devices that collects and blocks the passage of air bubbles into the main system. For instance, bubble traps are fabricated by molding a well into the design or cutting it out after the curing process (Eddington, 2006b); adding barriers that act like as a sieve on a top layer above the fluidic path (Sung and Shuler, 2009a); using a 'bubble sink' which uses surface tension to capture air bubbles (Meng et al., 2006); using hemispherical wells or cylindrical chambers that trap bubbles by buoyancy (Kang et al., 2010; Zheng et al., 2010b); applying a temperature gradient in continuous flow (Selva et al., 2010) and using a wide channel right above of a narrow channel since bubbles tend to move to the wider channel due to surface tensions (Kohnle et al., 2002). However, one limitation of this approach is that bubbles are not completely removed from the system and traps can be filled completely and allow additional bubbles into the system which can have devastating effects. On the other hand, microfluidic debbublers are a more efficient method because it removes the bubbles out from the device (Kang et al., 2008c). There is a variety of mechanisms used to remove bubbles such as using ultrasonic induced cavitation (Yang et al., 2002), using the permeability of PDMS membranes (Skelley and Voldman, 2008b; Karlsson et al., 2013), porous hydrophobic acrylic copolymer membranes (Xu et al., 2010a), porous hydrophobic poly (tetrafluoro ethylene) (PTFE) venting membranes (Liu et al., 2011; van Lintel et al., 2012c). Additionally, including structures in the mold to induce negative pressure such as vacuum channels for cell loading into culture chambers (Kolnik et al.,

2012) and vacuum suction ports for polymerase chain reaction (PCR) (Trung et al., 2010). In addition, there are other methods that utilized a combination of bubble traps and debbublers. For example, connecting a bubble trap with a vacuum source through a PDMS member (Zheng et al., 2010c), capturing bubbles using ring-shaped corral as a trap and applying negative pressure through a permeable PDMS membrane (Skelley and Voldman, 2008c) and using a bigger trap like a reservoir with posts to support the PDMS membrane (Johnson et al., 2008), or a cylindrical trap chamber that traps bubbles and remove them through PDMS permeability of a vacuum chamber (Lochovsky et al., 2012c). The common aspect of all of these systems is that they require external vacuum sources or air compressors, complicated fabrication procedure and setup expertise (Wang et al., 2012d). In addition, if the aspect ratio of the channel is not controlled, the vacuum pressure applied can cause the channel to collapse. Another method used for bubble removal is based on the PDMS solubility. PDMS devices are submerged in the solution of interest and then placed on a vacuum chamber so that air escapes through the inlet or outlets as soon as the atmospheric pressure decreases. Once the pressure is normalized, the device is completely filled. (Monahan et al., 2001b). Other devices have used the same principle of absorbing air through degassed PDMS for dispensing liquid in microarrays (Zhou et al., 2007) and cell loading (Luo et al., 2008). However, the problem with this method is that the whole PDMS device needs to be in a vacuum chamber and there are certain parameters to consider such as PDMS thickness, channel geometry, degassing time, PDMS exposure area and idle time at atmospheric pressure before loading (Liang et al., 2011). Another problem is that the majority of bubble removal systems are used for channels greater than 100 μm. None of these systems addresses

channels with a width in the range of 15 to 50 μm which are very sensitive to any contact and are mostly used for blood flow. In addition, the microfluidic device with gas-liquid interphase are the most susceptible to bubble formation. In general, these devices are made from bonding two PDMS layers, one layer for liquid flow and the other for gas flow. These devices are known to be challenging to handle due to the bubble formation caused by this interphase. However, this gas layer not only allows the gas to permeate, but it can also work as an extraction tool. This approach is sometimes overlooked and completely ignored by the people operating the device. For that reason, we proposed a different mechanism to remove air bubbles using a converging-diverging nozzle which induces the Venturi effect.

### 1.4 Venturi Effect

The Venturi effect was discovered by Giovanni Venturi. A converging-diverging nozzle or also referred to as ‘de Laval’ nozzle can induce the Venturi effect by increasing the pressure difference between the inlet and outlet pressures. This effect has been widely used in Venturi meters which measure the flow speed of fluids; in a flying airplane when the wind flows faster above the wing causing an upward lift and spray nozzles which release compressed air through a constriction and the pressure drop forces out the liquid. In order to use the Venturi effect, the device requires an inlet region, a converging section, a narrow channel or throat linked to a sidearm, a diverging section and an outlet region open to the atmosphere. When a fluid flows into a narrow constricted channel, its velocity increases which leads to a pressure drop in order to keep the mass flow rate constant. Therefore, pressure from the atmosphere is driven towards the throat which is the narrowest part of the device to compensate for the loss of pressure as seen in figure 2.

For example, when a liquid flows from a converging to diverging channel, it causes an increase in its kinetic energy. As a result, it leads to a pressure drop in order to maintain the total energy constant, according to the Bernoulli principle seen in equation 2 (Perdigones et al., 2010a).

$$p + \frac{1}{2}\rho v^2 = constant \qquad \text{Eq. 2}$$

where p is the pressure (kg/m·s$^2$), ρ is the density of the fluid (kg/m$^3$) and $v$ is the velocity of the fluid (m/s). Although the Venturi effect also occurs when the fluid is a gas or a compressible fluid, an important aspect to remember is that the density of the gas is dependent on the pressure and temperature, so it can not be assumed to be constant. Another aspect to consider is when the flow is choked. In most cases, when the pressure difference is low, the flow accelerates the convergent section with a subsonic speed until it reaches its maximum speed at the throat and then, starts decelerating from the divergent section into the ambient as a subsonic jet. However, when the pressure difference is high, the flow at the throat can only reach a Mach number of 1 which means that the fluid velocity is the same as the sound velocity in that medium. Therefore, the fluid velocity is fixed at the throat because it is the section with the smallest cross-sectional area. The flow goes from subsonic to sonic at the throat, which causes a choked flow. Another explanation for this effect is when you consider the flow at the throat as a turbulent jet. The gas leaves the throat as a turbulent jet that expands, based on the jet radius. This effect causes the gas to enter the vacuum tube which increases the pressure.

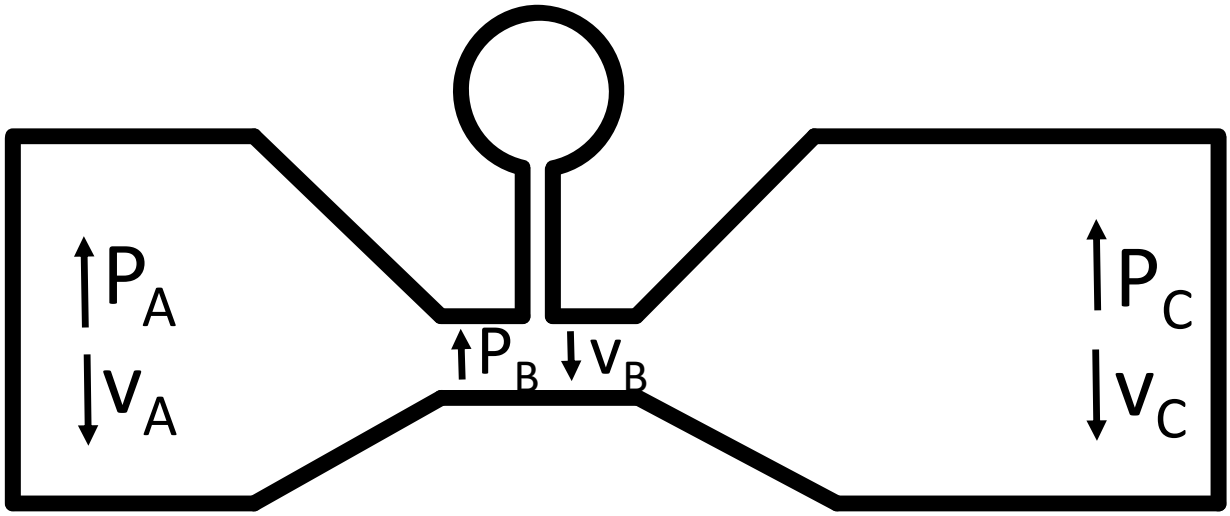


Figure 2. Representation of the Venturi effect. At the inlet, the initial pressure ($P_A$) is high, but the velocity of the fluid ($v_A$) is low. At the throat, the velocity increases ($v_B$), but the pressure decreases ($P_B$). At the outlet, the outlet pressure increases ($P_C$), but the velocity decreases ($v_C$).

In microfluidics, the Venturi effect has been analyzed and used for different applications due to its benefits such as simple fabrication, inexpensive cost and precise control of a range of negative pressures (Perdigones et al., 2010b). For instance, the Venturi effect has been applied for several applications such as controlled liquid aspiration (Perdigones et al., 2010c), a gathering tool for gastrointestinal juice sample (Koo et al., 2011), interstitial fluid transdermal extraction and fluid manipulation(Yu et al. 2012a), droplets generation (Hettiarachchi and Lee, 2008), and microregulator of pressures (Chang et al., 2007). In addition, its vacuum efficiency has been measured by changing different parameters such as divergent angles, convergent angles, width and length of the throat channel (Yu et al., 2012b). However, this effect has never been used for a microfluidic bubble removal system. For that reason, we propose a bubble debubbler that uses the converging-diverging nozzle as the vacuum source. Not only will this improve the portability of the system, but it can also work with previously mentioned bubble traps as well as debubblers. This bubble extraction system is ideal for the microfluidic devices with

gas-liquid interphases because those are more susceptible to bubble formation than any other microfluidic device due to the permeability of PDMS. Most of these devices have multiple layers which can form air bubbles. Moreover, the ability to adjust a wide range of negative pressures can be used to control the bubbles size.

# CHAPTER 2: MATERIALS AND METHODS

## 2.1 Devices Fabrication

For the system to be functional, it is necessary to fabricate a device which will generate negative pressure based on the Venturi effect and a microfluidic device that has a bubble formation problem. For the fabrication of the converging-diverging nozzle and the network model device, standard photolithography techniques followed by the soft lithography process were performed for each of the different components. For this experiment, two different microfluidics elements were fabricated and used which were the network model device and the external vacuum source. After the bubble removal quantification, we tested the system using different channel patterns.

### 2.1.1 Network Model Device

Although most microfluidics channels are between 30-300 μm (Panigrahi, 2015d), there are several studies that reported using devices with channel networks that resembled the vascular networks. These channels can range from 5 to 20 μm which can be very sensitive to bubble formation. For that reason, a network model device was chosen as a testing device. The network model device consisted of two PDMS layers that are bonded by plasma treatment. The two layers are the gas chamber and a membrane which contains the parallel channels. In order to make both PDMS layers, each layer requires a mold made by photolithography techniques. However, the fabrication for the parallel channel mold will require a special fabrication procedure due to its features dimensions.

#### 2.1.1.1 Network Model Membrane

Although the photolithography process was described in section 1.1.2, certain modifications can be done to improve the mold's resolution. These protocol modifications can be spinning a base layer on the wafer or changing the exposure source. The mold for the parallel channels was done by dehydrating a 76.2 mm diameter silicon wafer (University Wafer) with acetone, IPA and deionized (DI) water and drying it using an air gun followed by baking for 2 minutes. A negative photoresist, SU-8 2015 (MicroChem) was spun on the dehydrated silicon wafer at 3500 rpm for 30 seconds using a spinner (Laurell Technologies Corporation, North Wales, PA). Once the silicon wafer was coated with SU-8, it was baked at 95°C for 3 minutes and exposed to UV light at an intensity of 100% (664 mW/cm$^2$) for 20 seconds without using any photomask. Then, the SU-8 coated wafer was baked at 95°C for 5 minutes. This base layer enhances the deposition of pattern designs with small features. After it cooled down, another layer was spun using the same procedure until the exposure step. In this step, the wafer was exposed using a maskless lithography system called μPG 101 (Heidelberg instruments, Mikrotechnik GmbH) which has a laser that exposes standard photoresists with high precision and resolution. The design of the network model membrane was done using AutoCAD loaded to the computer connected to the μPG 101. The design consisted of a series of 55 parallel channels with a width of 15 μm and a length of 33 mm separated by a distance of 50 μm. The channels are connected at the beginning and at the end to two chambers which is for the inlet and outlet holes. These chambers are 5 mm long and 3.5 mm wide. The wafer was exposed at least two times with a power exposure of 18 mW at an intensity of 100% with a energy factor of 4x each time and then, baked at 95°C for 5 minutes. The coated

wafer was developed afterwards using a SU-8 developer for 2 minutes, rinsed with IPA and dried with an air gun before placing the mold in a silanized chamber for at least 2 hours. The achieved height of the mold was 12 μm. After that, a mixture of PDMS (Sylgard 184 Silicone Elastomer; Dow Corning Corp., Midland, MI) with curing agent using a 10:1 mixing ratio was prepared using a planetary centrifugal mixer called AR-100 (Thinky Corporations, USA). Around 10 grams of the PDMS mixture were spun at 800 rpm to achieve a 100 μm thick membrane. Then, it was placed on a desiccator for 5 minutes and baked at 85°C for 15 minutes.

#### 2.1.1.2 Gas Chamber

The design of the gas chamber was done using AutoCAD and a photomask (Fineline imaging) was printed with the desired design. The design consisted of a rectangular area of 33 mm length and 5 mm wide with two rows of 400 μm diameter posts separated with a distance of 1.8 mm between them. The inlet and outlet holes are connected to this area on the diagonally opposite corners. For the fabrication of the gas chamber, a layer of SU-8 2050 was spun on a dehydrated 100 mm diameter silicon wafer at 1500 rpm for 30 seconds followed by a bake at 65°C for 5 minutes and then, at 95°C for 30 minutes. The photomask was exposed on the silicon wafer at a 100% intensity (664 mW/cm$^2$) for 60 seconds and then, baked at 65°C for 5 minutes and 95°C for 12 minutes. After that, the mold was developed with SU-8 developer for 10 minutes followed by the silanization process. The mold achieved an average height of 150 μm measured using an interferometer. Once the gas chamber mold was fabricated and silanized, then a mixture of PDMS and curing agent was prepared using the same mixing ratio described previously. Around 35 grams of PDMS mixture were poured into a squared petri dish with

the mold on it and placed on a desiccator for 30 minutes before baking it at 85°C for 1 hour and 30 minutes. One of the advantages of this process is that you can create multiple layers with one mold as seen in figure 3. Each PDMS gas chamber layer was removed using a standard razor and the inlet and outlet holes were punched using a 11-gauge size (2.30 mm).

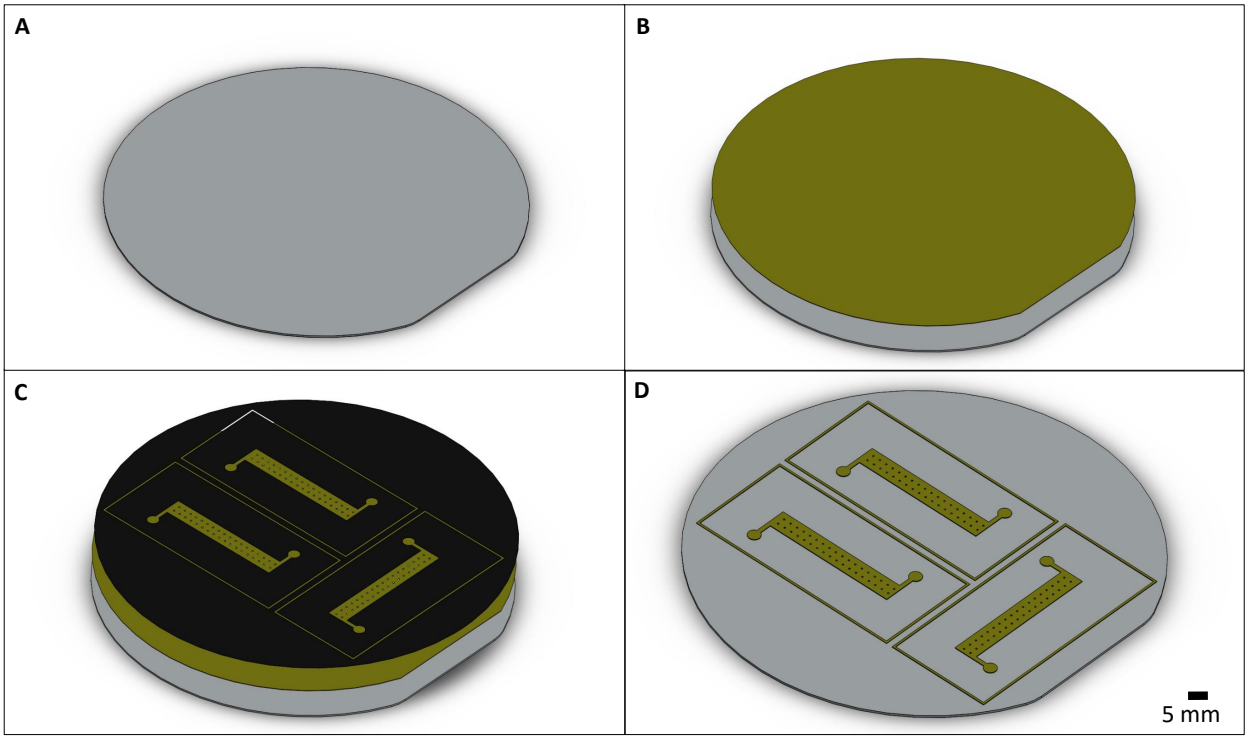


Figure 3. Fabrication process of the gas chamber mold. (A) A 100-mm diameter silicon wafer is dehydrated and cleaned. (B) A negative photoresist (SU-8 2050) is spin coated over the 100 mm diameter silicon wafer and bake. (C) A photomask with the specific design is used for the UV exposure. (D) the mold is finalized after the SU-8 developer is used to remove all the unexposed regions.

#### 2.1.1.3 Assembly

During the assembly of the network model device, a PDMS gas chamber layer was plasma treated as well as one of the PDMS membrane using a corona discharge (Electro Technic Products, Chicago, IL). The gas chamber layer was bonded directly above the PDMS membrane. Once the membrane was bonded to the gas chamber, the mold with

the PDMS gas chamber was baked at 85°C for 15 minutes to enhance the bonding. After that, the PDMS gas chamber bonded to the network channel membrane was removed and the inlet and outlet holes for the network channels were punched throughout the top PDMS layer using a 13-gauge size (1.83 mm). Finally, it was bonded to a 25.4 x 76.2 mm glass slide (Fisher Scientific) using the corona discharge and baked at 85°C for 5 minutes to enhance the bonding. Schematics of the final assembly can be observed in figure 4. Each network model device fabricated is stored on a petri dish for the experiments.

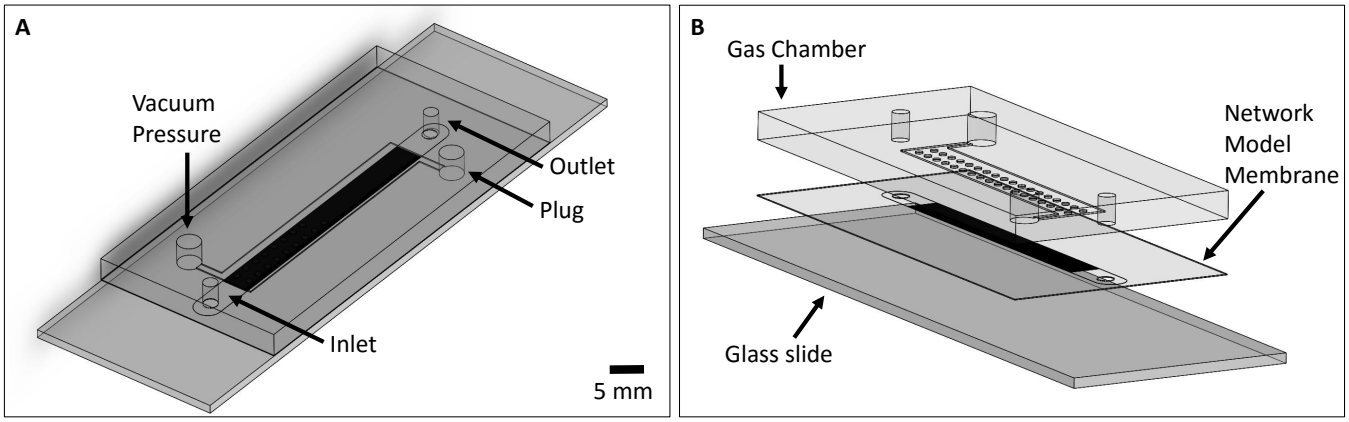


Figure 4. Assembly of the network model device. (A) Both PDMS layers are bounded to the glass slide through plasma treatment. (B) An exploded view of the device which shows the gas chamber, network model membrane and the glass slide (top to bottom).

### 2.1.2 Converging-Diverging Nozzle Device

#### 2.1.2.1 Fabrication & Assembly

The vacuum source mold was fabricated by spinning SU-8 2150 at 630 rpm for 30 seconds on a dehydrated 100-mm diameter silicon wafer. The SU-8 coated silicon wafer was baked at 65°C and 95°C for 6 and 98 minutes, respectively. The design of the converging-diverging nozzle was made using AutoCAD and a photomask with the design was printed. The converging-diverging nozzle used for this project covered an area of 200 $mm^2$ with an average height of 300 μm across all sections. The dimensions of the design were 30° for the convergent angle, and 3.6° initially and then, 40° for the divergent

angle, the width of the throat is 30 μm and expands until it reaches 100 μm, the vacuum output channel is 2 mm wide and 4 mm long. The photomask containing the design was exposed into the SU-8 coated wafer at 100% intensity for 30 seconds and later on, baked at 65°C and 95°C for 5 and 26 minutes, respectively. Finally, the coated wafer was soaked using a SU-8 developer for 10 minutes. Once the master mold is finalized, a mixture of PDMS with curing agent was prepared, poured into the mold and cured with the same procedure described previously. Once the vacuum source was cured, the PDMS layer was removed using a razor. An 11-gauge size (2.30 mm) was used to make the inlet and outlet holes. In addition, a small cut on the outlet section of the device is done so that it is open to the atmosphere. Finally, the PDMS layer is bounded to a glass slide using a corona discharge and baked to enhance the bonding.

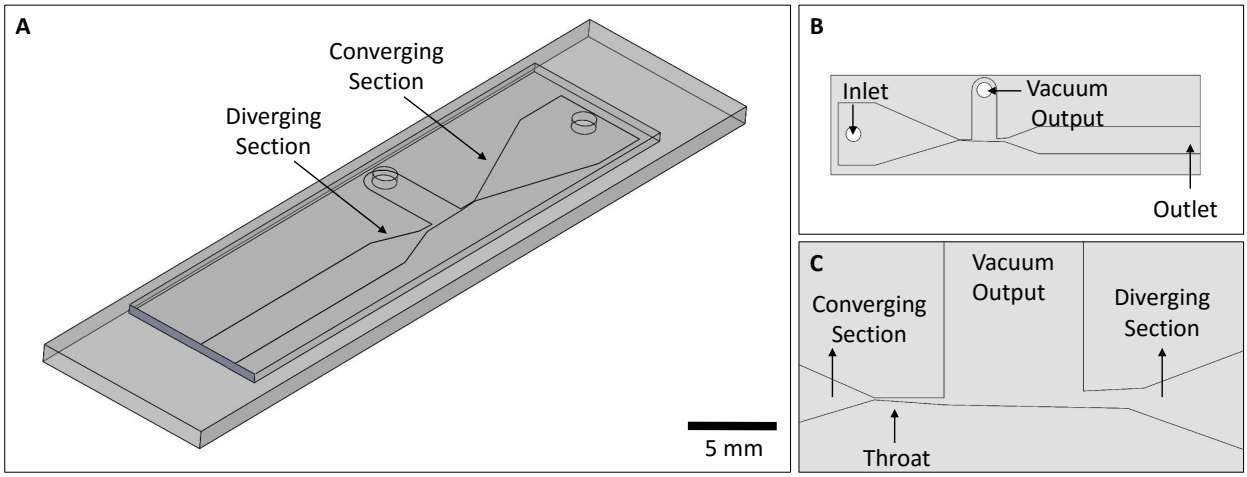


Figure 5. Schematics of the converging-diverging nozzle. (A) The microfluidic device which consists of the PDMS layer bounded to a glass slide. (B) Top view of the PMDS layer showing the inlet, outlet and vacuum holes and (C) Zoom-in of the nozzle area

### 2.1.3 Alternative Channel Design Devices

In order to test the performance of the bubble removal system on different channel designs, two channel designs that contained a series of triangular and circular structures

were used instead of the parallel channel membrane. Therefore, most of the fabrication protocol used for the network layer was followed with changes on the channel design. The designs were previously done using AutoCAD and uploaded to the μPG 101. They consisted of two separate 50 μm wide channels, each channel had either the loop or the triangular structures. The loop channel has a series of 11 loops with an inner diameter (ID) of 400 μm and outer diameter (OD) of 450 μm, connected to a main channel of 50 μm wide and 43 mm long. The triangular channel consisted of a series of triangular structures with an angle of 30 degrees attached to a main channel through the base. Therefore, the final height achieved by the mold was 12 μm for both channels. Because of the ease of fabrication, one mold which had both channel designs was fabricated and silanized. Then, a PDMS membrane was spun on the mold and assembled with a gas chamber using the same procedure as the network membrane.

**2.2 FITC Solution Preparation**

Once the devices are assembled, a solution of fluorescein isothiocyanate (FITC) is used as the fluid flow in the parallel channel device. The reason for using a FITC solution was because the fluorescence provides a better visualization of the air bubbles in the microchannel. The length of the bubble can be defined as the distance from one fluorescent side to the other which can be measured by a specialized software. The solution was prepared by dissolving FITC (Sigma Aldrich) in dimethyl sulfoxide (DMSO) and achieving a concentration of 11.6 mM for the stock solution. Then, the mixture was diluted four times, leading to a final concentration of 2.9 mM. In early experiments, there were problems with the FITC solution because it was not dissolving completely into the

DMSO. Additional dilutions ratio was tested to see whether this change affected the results, but not a significant difference was observed, so this dilution was kept.

**2.3 Experimental Setup**

A syringe was loaded with the diluted solution and used to fill 1/4 long of the total length of the channels through gravity driven flow and using a tygon tubing with 0.51 mm ID and 1.52 mm OD (Cole-Parmer, Vernon Hills, IL). Using the same procedure, a 1/4 length of the channels was filled, but from the opposite side of the device. The reason for doing this is to obtain several bubbles located in the middle of the device that were surrounded by the FITC solution which will be used to quantify the bubble removal rate of the converging-diverging nozzle. The nozzle requires an initial pressure which is provided by flowing gas from a pressurized gas tank. For our purposes, a nitrogen gas (PraxAir), but any type of pressurized gas tank can be used for our purposes. The pressurized nitrogen gas tank was connected to a rotameter (Omega Engineering, Inc., Stamford, CT) which was also connected to a FMA-A2306 electronic mass flowmeter (Omega Engineering, Inc., Stamford, CT). The electronic flowmeter measured the gas flow going into the converging-diverging nozzle and it ranges from 0 to 1641 standard cubic centimeters per minute (sccm). As the flow increases, the initial pressure going to the converging-diverging nozzle increases. Depending on the flow, a variety of negative pressures was generated which had an effect on the rate of bubble extraction. The vacuum outlet was connected to the gas chamber of the device using a tygon tubing with a 1.58 mm ID and 3.17 mm OD (Cole-Parmer, Vernon Hills, IL). At the other outlet of the gas chamber, a plug (McMaster) was connected to maintain the negative pressure on the gas chamber. As soon as the nozzle was connected, the bubble located in the middle of

the device started to shrink at different rates, depending on the negative pressure being applied to the gas chamber.

As soon as whole bubbles were observed on the fluid channels, a digital CCD camera connected to a fluorescence microscope acquired a series of frames using an image analysis software called Metamorph. The frames captured the bubbles being removed from the moment the vacuum outlet was connected to the gas chamber. Each frame at known time intervals was analyzed using ImageJ to enhance the contrast followed by volume quantification of the air bubbles using a MATLAB code (See Appendix for the complete code). The MATLAB code measured the length of a single air bubble surrounded by the FITC solution. By knowing the width and height of the channels, then the volume was calculated at each known time interval which subsequently, was used to plot the bubble volume decay over time. In order to make a comparison between the different applied negative pressures, the removal rates needed to be calculated since the bubble volumes were not uniform. By using a linear approximation, the removal rates of at least three different bubbles were calculated at each of the specific negative pressures.

### 2.4 Test Using Different Channel Designs

Another aspect from the bubble removal system to be tested was its performance on different channel designs. Certain channels have structures with acute angles, sharp corners or loops which are known to have dead volumes. These air bubbles are difficult to remove so the device has to be placed on a desiccator for several minutes or used any of the removal techniques previously described. Therefore, we predict that if the channel design is exposed to the gas chamber layer, any air bubble located on the fluidic channel will be removed independent of the channel design. Once the devices were assembled,

water was flowed in one of the inlets and an air bubble was formed as seen on figures 1 (B&C) at 0 seconds. After applying negative pressure to the gas chamber, a series of pictures were acquired and analyzed using the same procedure previously mentioned. This experiment demonstrated the application of the Venturi effect as a bubble removal system using different channel designs.

## CHAPTER 3: RESULTS

### 3.1 Performance of the Converging-Diverging Nozzle

The first experiment performed was to measure the range of negative pressures generated by the converging-diverging nozzle. A schematic diagram of the setup for this experiment is seen in figure 6. The initial pressure applied on the inlet port of the converging-diverging nozzle was regulated by a rotameter connected to a nitrogen gas tank. This initial pressure and the output vacuum pressure were measured using a pressure sensor (40PC100G2A, Honeywell Sensing and Control) and a vacuum pressure sensor (40PC015V2A), respectively. The collected data was sent to an analog input module (NI 9205) connected to a data acquisition interface (NI cDAQ-9174).

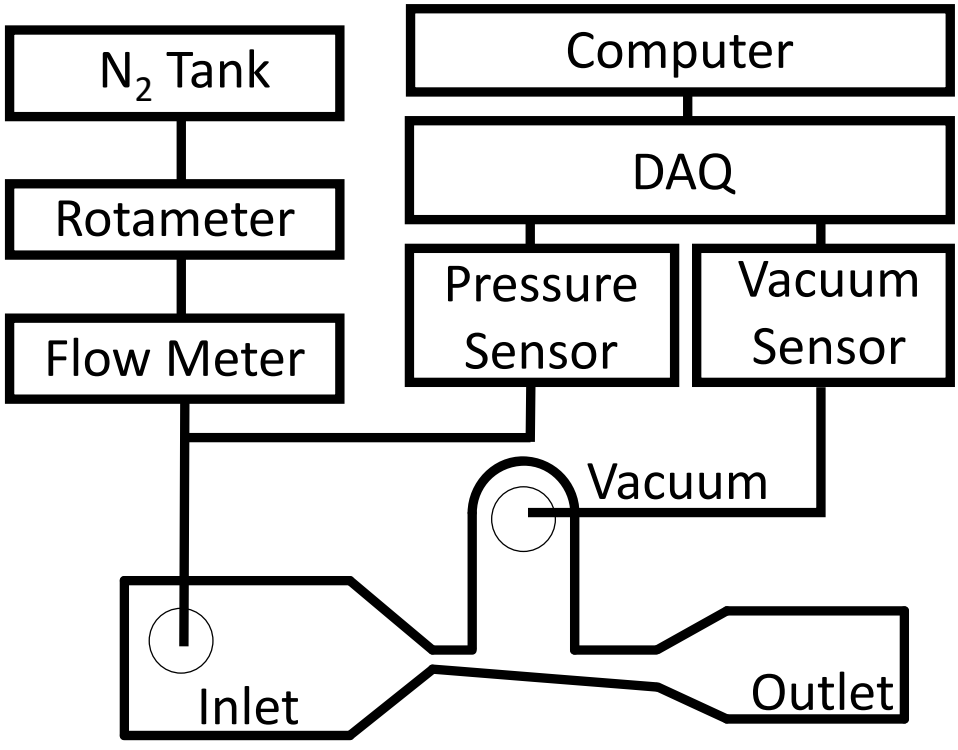


Figure 6. Experimental setup for the vacuum pressure measurements of the converging-diverging nozzle.

Using this experimental setup, different external pressures were generated which corresponded to a wide range of negative pressure. The resulting plot is seen in figure 7 which shows that for the converging-diverging nozzle, the minimum negative pressure achieved was -7.37 psi and it was achieved with an initial pressure of 32.3 Psi which represents a flow of 1100 standard cubic centimeters per minute (sccm).

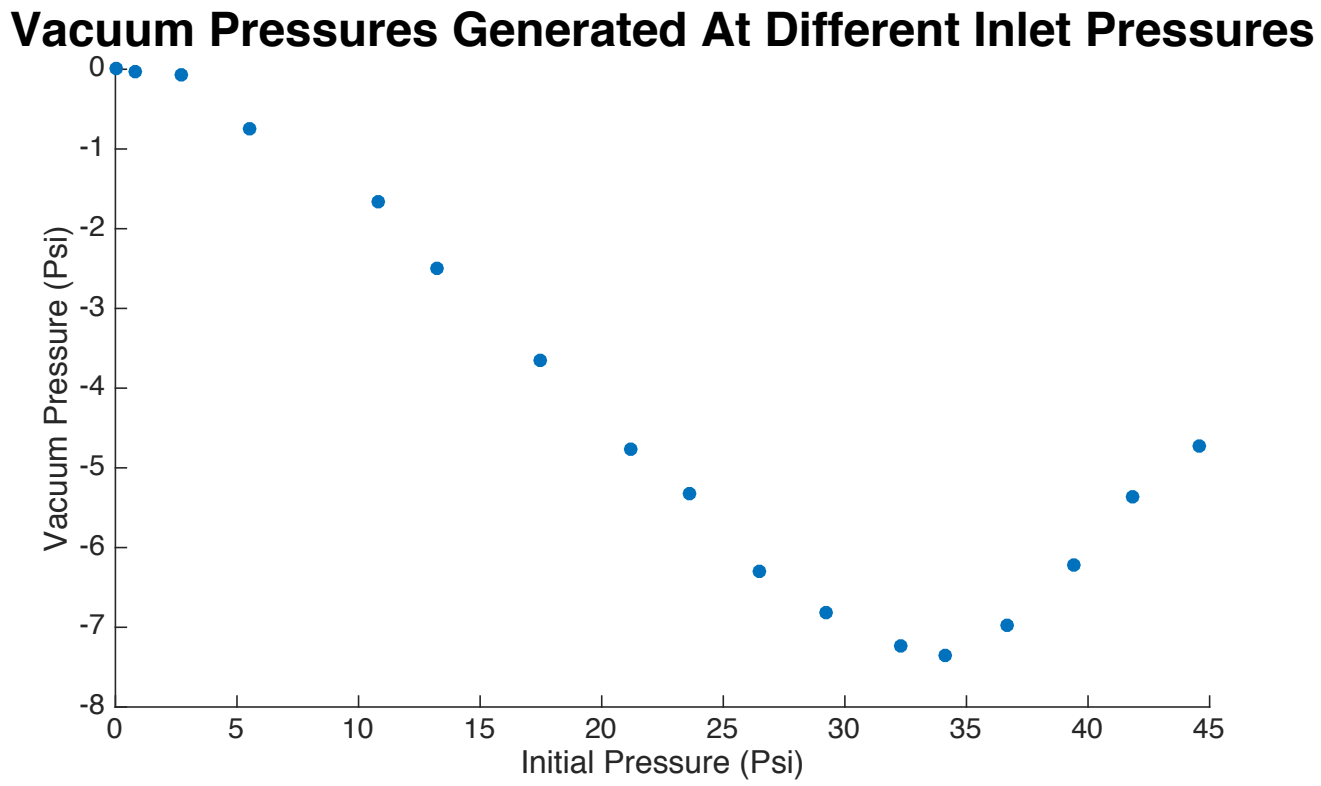


Figure 7. Performance of the converging-diverging nozzle at different inlet fluid flows.

For the Venturi effect to occur, it requires a minimum initial pressure of around 5.5 psi which is close to the 300 mbar (4.3 psi) that Perdigones et al. reported in his device. If the flow increases after that, then the negative pressure starts to increase because of the choked flow and the turbulent jet flow described in section 1.4. A choked nozzle is when the fluid reaches a Mach number of 1 which is the ratio between the fluid velocity and the sound speed. The velocity of the fluid increases because of the pressure difference,

however it reaches a limit at the smallest cross sectional area. Therefore, the fluid velocity at the throat will not go any faster even if the pressure difference increases. Based on the increasing vacuum pressure with an input pressure of 5.5 to 32.3 psi, a fair prediction that can be made is that the bubble removal rates should increase in a linear way.

### 3.2 Bubble extraction rate characterization

In order to quantify the bubble extraction rate, a single air bubble was generated by flowing the diluted FITC solution in both the inlet and outlet holes of the device consecutively. Once a single bubble is formed at the middle part of each channel, then, it can be removed by applying constant negative pressure generated by the converging-diverging nozzle. A complete setup can be observed in figure 8, where a tubing from the nitrogen gas is connected the converging-diverging nozzle is connected to the gas chamber of the device and a plug is connected to the other end. Figure 9 shows the air bubbles formed in each of the channels and how they vanished 48 seconds after applying -5.5 psi to the gas chamber.

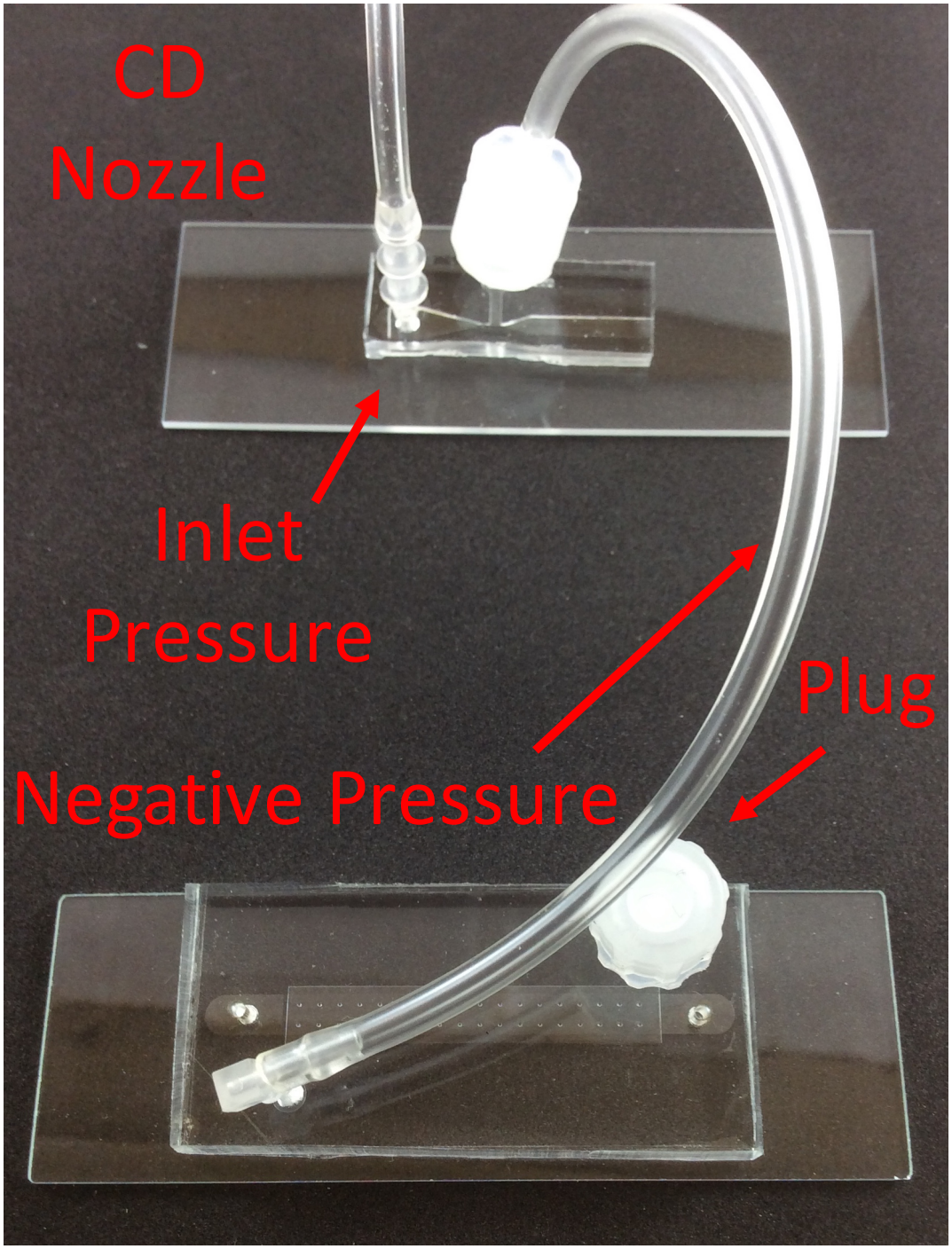


Figure 8. Experimental setup of the converging-diverging (CD) nozzle and the network model device. The inlet pressure was provided by a nitrogen gas tank and the pressure was controlled by a rotameter.

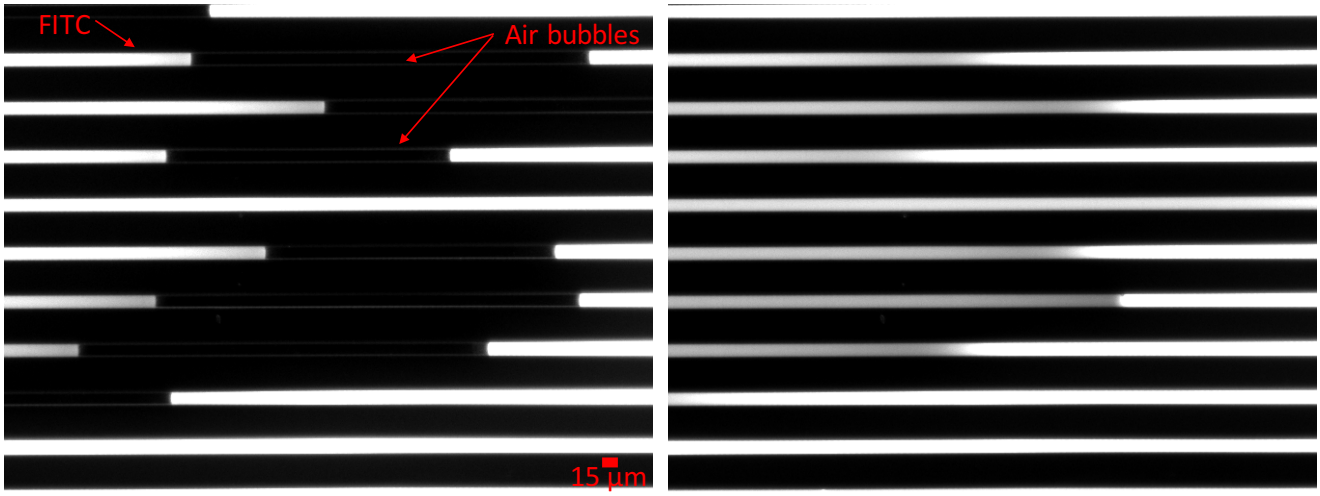


Figure 9. Schematic of air bubbles in FITC solution. The channels are 15 µm wide filled with FITC before and after the negative pressure was applied. Pictures acquired using the 10X objective.

The nitrogen flow input an initial pressure to the converging-diverging nozzles which generated a constant vacuum pressure. After analyzing a time series at a specific negative pressure, the bubble volume decayed over time is observed. Figure 10 shows the volume of several air bubbles being removed at different positive pressures which demonstrated that as the negative pressure decreases, the bubble shrinks faster.

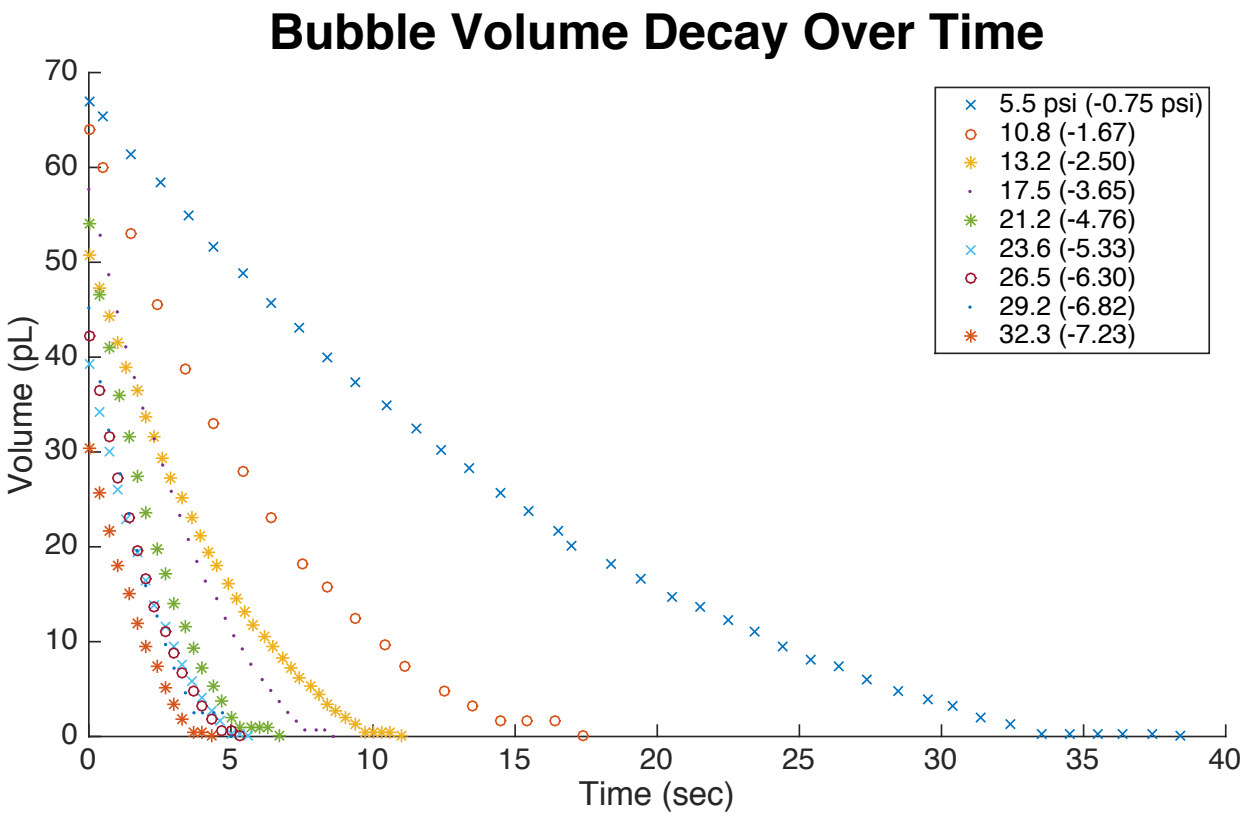


Figure 10. The volume of air bubbles surrounded by FITC solution decreased over time at different positive pressures.

As soon as we analyzed the volume decay of multiple bubbles, then the removal rates are quantified by a linear approximation of the slope. The average is taken from at least three bubbles at each of the negative pressure applied. In figure 11, the average rates are plotted with their corresponding negative pressures, and the highest rate achieved was 9.84 pL/s with a vacuum pressure of -7.37 psi which corresponds to the minimum negative pressure achieved by the converging-diverging nozzle. As mentioned before, this negative pressure was generated by applying 32.3 psi at the inlet pressure of the converging-diverging nozzle.

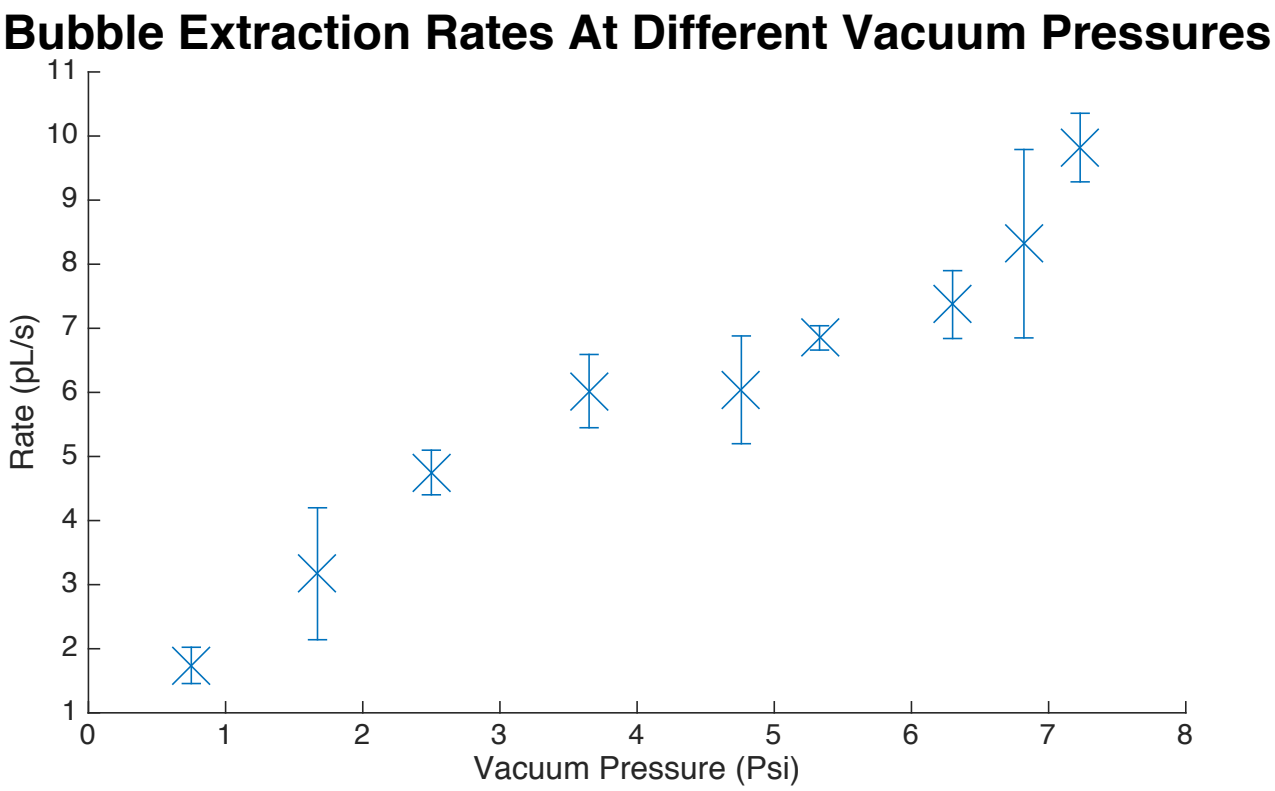


Figure 11. Bubble removal rates at different vacuum pressures. As the negative pressure increases, so does the bubble removal rate.

Any initial pressure lower than 32.3 psi will increase the minimum negative pressure achieved. The reason for this increase is due to the shock wave, causing a pressure increase. At this point, the flow reaches its maximum speed because it is the minimum cross sectional area. This effect is expected to happen due to the converging-diverging nozzle design.

### 3.3 Performance using alternative channel designs

Although the bubbles were removed on the parallel straight channels within seconds, microfluidics channels tend to have more complicated designs. For that reason, the bubble removal system was tested on two different channels, as seen in figure (1B and 1C). Bubbles are formed on channels with designs that have small angles and loop

shape structures. By applying the negative pressure from the converging-diverging nozzle, it was observed that the bubbles are removed in a matter of a few minutes for both of these designs. This is understandable, since the channel width is bigger and also the design of the channel is different as well. Figures 12 and 13 shows the performance of the converging-diverging nozzle by applying a vacuum pressure of -0.75 psi using different channel geometries.

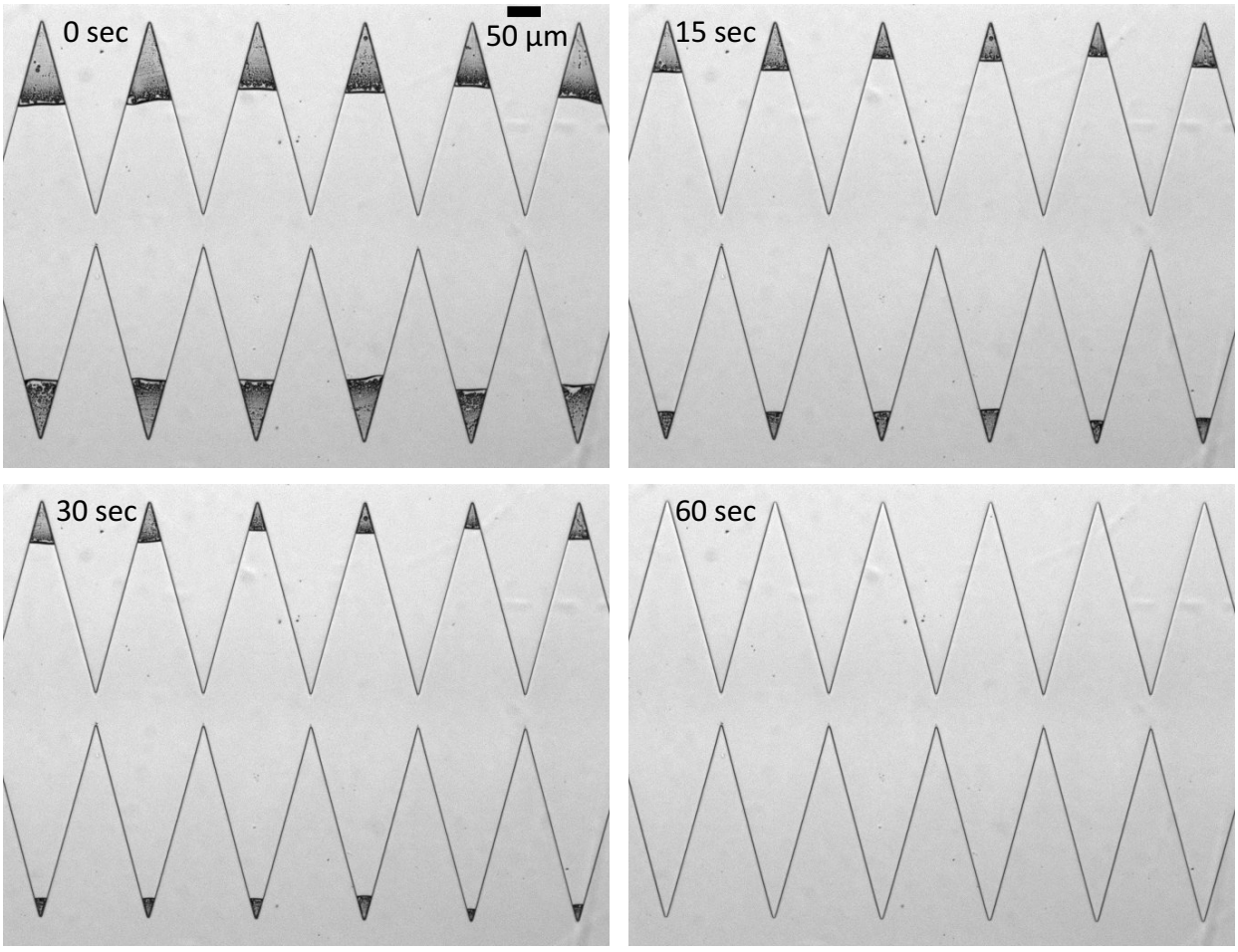

Figure 12. Progression of a bubble removal on a triangular channel. Each figure is taken at 0, 15, 30, 60 seconds, respectively.

In addition, another problematic channel design is with the use of loops that creates bubbles.

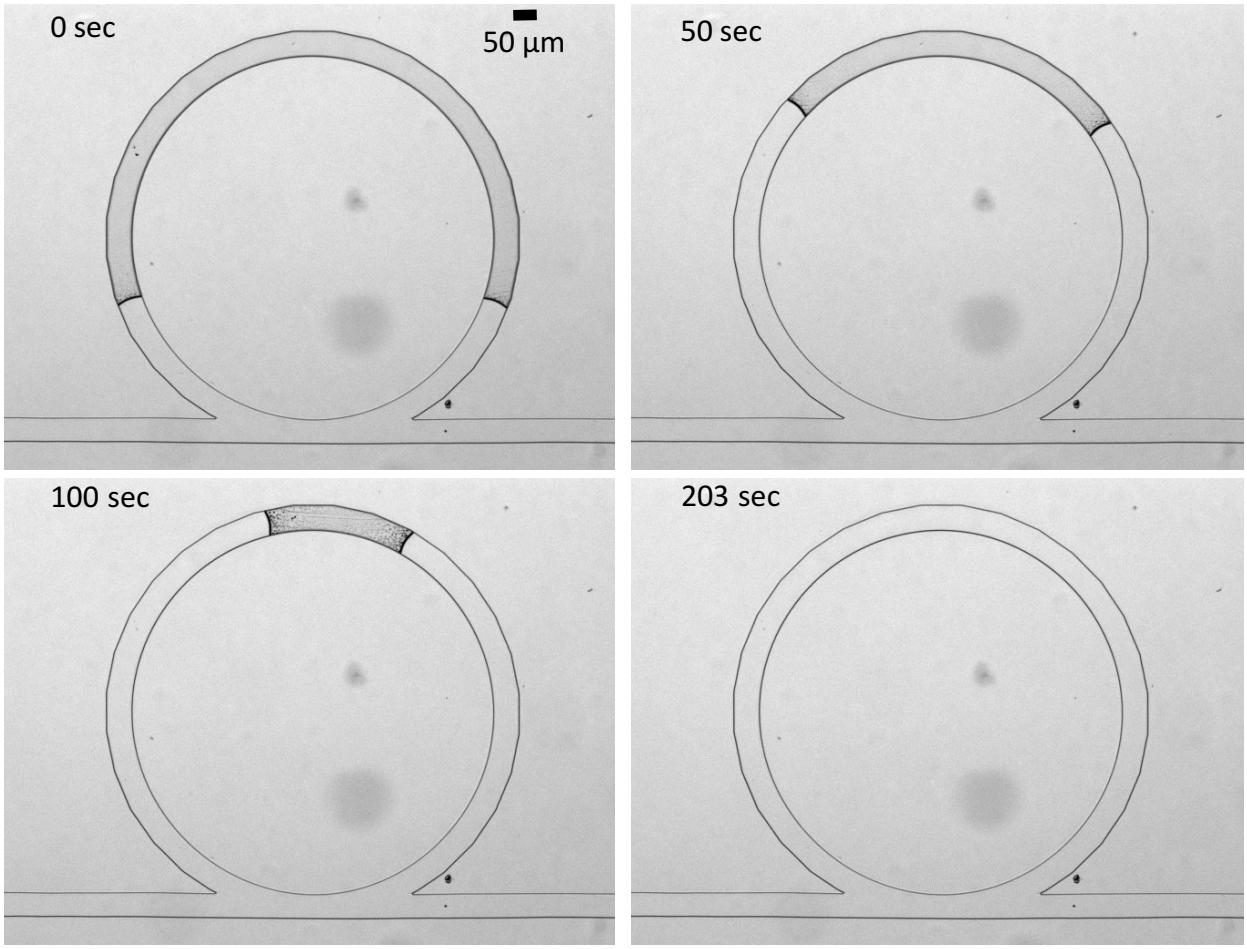

Figure 13. Progression of a bubble removal on a loop channel. Each figure is taken at 0, 50, 100, 200 seconds, respectively.

These results serve as a proof of concept that the geometry of channel does not affect the performance of the converging-diverging nozzle.

# CHAPTER 4: DISCUSSION

## 4.1 Advantages of the Bubble Extraction Tool

Until now, the Venturi effect was never used as a vacuum source for a microfluidic bubble removal system. Not only has microfluidics been able to replicate this effect at the microscale, but also provide researcher with other benefits such as ease of fabrication, portability and user-friendliness. Most of the commercially available bubble removal systems like Systec Debubbler series (BioTech AB, Sweden) and the Omnifit bubble trap work with dead volumes greater than 1 mL which is a huge volume compared to the volumes used in microfluidics (van Lintel et al., 2012d). Not only are these systems more expensive than the previously mentioned approaches, but they also need the constant of replacements parts like PTFE membranes. Other bubble removal systems used different approaches such as bubble traps or a combination of traps with debubblers. These systems used a variety of materials such as hydrophobic membranes and vacuum channels. For example, some removal systems have rates of 0.14 µL/min (Lochovsky et al., 2012d), 0.01 µL/s (Sung and Shuler, 2009b), 0.0023 µL/s (Skelley and Voldman, 2008d) 0.0005 µL/s/mm$^2$ (Xu et al., 2010b), but they all used vacuum pumps which provide pressures of -97 kPa relative to atmospheric. In addition, they used channels with large cross-sectional areas compared to the channels used in this project, but none of them applied their bubble removal system in smaller channels or thinner membranes which are more sensitive to collapse when that amount of negative pressure is applied. Another reason for the use of vacuum pumps is the thickness of the actuation membrane. Several systems have reported using 300-200 µm thick PDMS membranes which are more stable than thinner membranes, but at the same time can lead to slower removal

rates. Although thinner membranes are hard to cure, we have shown a way to handle 100 μm thick PDMS membranes. For those reasons, a converging-diverging nozzle can be more effective compared to other methods. Although the removal rate is slower compared to other methods (9.84 pL/s), it avoids the collapse of any membrane in the microfluidic device. Another aspect to mention is the portability and functionality of the converging-diverging nozzle. Even though a gas tank was used, as the source of initial pressure, other sources can be used such as a bicycle pump. These advantages add on the ease of fabrication and user friendliness.

In order to determine the steady-state flux across a thin membrane, a predicted bubble removal rate through a PDMS membrane can be calculated by (Kang et al., 2008d):

$$-\frac{dV}{dt} = \frac{PA(p_2 - p_1)}{b} \times \frac{T}{273} \times \frac{76}{P_{atm}}$$

where $P$ is the PDMS permeability (1.92 x $10^{-15}$ $m^2$ $s^{-1}$ $Pa^{-1}$), $p_2$-$p_1$ is the difference between the feed pressure and the permeate pressure (50.8 KPa), $b$ is the membrane thickness (1x$10^{-4}$ m), $A$ is the area covered by the PDMS membrane where the bubble is eliminated (1.65 x $10^{-4}$ $m^2$), $T$ is the temperature (273 K), and $P_{atm}$ is the atmospheric pressure (76 cm Hg). Assuming room temperature and normal atmospheric pressure, the removal rate is 0.1609 μL/s. This predicted removal rate is higher than what we measured and a possible reason to explain that is because the value used for the PDMS permeability does not reflect the permeability of the PDMS membrane used in the network model device. Another reason might be that the membrane thickness is less when it is

actuated. A higher steady state flux was also reported by Skelley and Voldman for their active bubble trap and debubbler.

Another positive effect of this system is that it has a faster effect than conventional removal systems such as a desiccator. Several microfluidic devices have been loaded with a solution and placed on a desiccator in order to remove air bubbles. However, this process is time consuming, since the vacuum chamber takes several minutes to degass all the air. For that reason, this system will be beneficial for any microfluidic device, but more importantly for PDMS devices that contain a gas-liquid interphase. Because of this gas-liquid interphase, these devices are the most susceptible for bubbles formation. Therefore, bubbles can be removed in those devices by applying the Venturi effect on their gas chamber. Several of the bubble removal systems requires complex bubble traps designs and a degassing site to remove those bubbles.

Although the converging-diverging nozzle may not be compared with a vacuum pump, it can still be useful. The negative pressures generated by the Venturi effect are more than acceptable for devices with dimensions similar to the network model device. There are different parameters that can be improve in our system, in order to obtain higher bubble removal rates which can be beneficial for devices with larger dimensions.

**4.2 Future experiments**

Certain modifications can be done to optimize this system. One of them will be to improve the vacuum efficiency of the converging-diverging nozzle by changing parameters such as decreasing the width of the throat, the diverging angle, converging angle and increasing the height of the nozzle. This vacuum efficiency improvement can lead to a higher bubble removal rates, but at the same time, it might cause the the gas

layer to collapse. Because of the portability of the nozzle, this can work with other bubble removal system by replacing the vacuum source. Another aspect to consider is the performance of this bubble system with constant flow of bubbles such as a bubble removal system for long-term cell culture. The converging-diverging nozzle is a simple, inexpensive, adjustable option to generate negative pressures. Although adding a gas chamber to a microfluidic device can be an extra step in the fabrication process, it substantially helps in the removal of air bubbles.

# CHAPTER 5: CONCLUSION

An alternative application of the Venturi effect generated by a converging-diverging nozzle is shown as the extraction force of a microfluidic air bubble removal system. Although there are currently several approaches to remove air bubbles, some of them require either additional chambers that act as bubble traps or large scale components such as vacuum pumps or air compressors as the extraction force. For that reason, a microfluidic converging-diverging nozzle was fabricated using PDMS which is coupled with a gas chamber to remove air bubbles. Gas chambers have demonstrated to permeate specific gases, but at the same time can be useful as bubble removal medium. By creating the converging-diverging nozzle, it improves the portability of other removal systems and it was shown to work specifically with devices that contain gas-liquid interphases. In order to quantify the rate of extraction, a solution of FITC was used to generate single bubbles in a network model device. Then, the volume of each bubble decay over time and the rates were calculated. Not only was the bubble extraction rate quantified, but it also demonstrated to be functional using complex channel designs as well as using different channel dimensions. However, there are different aspects of this system that can be improved such as bubble traps. In addition, the converging-diverging nozzle may even replace the vacuum pumps in other bubble removal systems. The expectations are that as the number of people working with microfluidic devices increases, the chances of encountering problems like unwanted bubble formation will also increase. Therefore, more improvements and innovations are still required for the current bubble removal systems.

## CITED LITERATURE


Anderson, Janelle R., Daniel T. Chiu, Rebecca J. Jackman, Oksana Cherniavskaya, J. Cooper McDonald, Hongkai Wu, Sue H. Whitesides, and George M. Whitesides. 2000. "Fabrication of Topologically Complex Three-Dimensional Microfluidic Systems in PDMS by Rapid Prototyping." *Analytical Chemistry* 72 (14): 3158–64. doi:10.1021/ac9912294.

Barker, Susan L. R., Michael J. Tarlov, Heather Canavan, James J. Hickman, and Laurie E. Locascio. 2000. "Plastic Microfluidic Devices Modified with Polyelectrolyte Multilayers." *Analytical Chemistry* 72 (20): 4899–4903. doi:10.1021/ac000548o.

Becker, Holger, and Laurie E. Locascio. 2002. "Polymer Microfluidic Devices." *Talanta* 56 (2): 267–87.

Betz, Amy Rachel, and Daniel Attinger. 2010. "Can Segmented Flow Enhance Heat Transfer in Microchannel Heat Sinks?" *International Journal of Heat and Mass Transfer* 53 (19–20): 3683–91. doi:10.1016/j.ijheatmasstransfer.2010.04.016.

Burns, M. A., B. N. Johnson, S. N. Brahmasandra, K. Handique, J. R. Webster, M. Krishnan, T. S. Sammarco, et al. 1998. "An Integrated Nanoliter DNA Analysis Device." *Science (New York, N.Y.)* 282 (5388): 484–87.

Campbell, Dean J., Katie J. Beckman, Camilo E. Calderon, Patrick W. Doolan, Rebecca M. Ottosen, Arthur B. Ellis, and George C. Lisensky. 1999. "Replication and Compression of Surface Structures with Polydimethylsiloxane Elastomer." *Journal of Chemical Education* 76 (April): 537.

Chang, Dustin S., Sean M. Langelier, and Mark A. Burns. 2007. "An Electronic Venturi-Based Pressure Microregulator." *Lab on a Chip* 7 (12): 1791–99. doi:10.1039/B708574E.

Choban, Eric R., Larry J. Markoski, Andrzej Wieckowski, and Paul J. A. Kenis. 2004. "Microfluidic Fuel Cell Based on Laminar Flow." *Journal of Power Sources* 128 (1): 54–60. doi:10.1016/j.jpowsour.2003.11.052.

Choi, Hyo-Jick, and Carlo D. Montemagno. 2006. "Biosynthesis within a Bubble Architecture." *Nanotechnology* 17 (9): 2198. doi:10.1088/0957-4484/17/9/020.

Colas, Andre. 2005. "Silicones: Preparation, Properties and Performance."

Denoual, Matthieu, Koh Aoki, Agnes Mita-Tixier, and Hiroyuki Fujita. 2003. "A Microfluidic Device For Long-Term Study Of Individual Cells." In . Squaw Valley, California USA.

Du, E., Monica Diez-Silva, Gregory J. Kato, Ming Dao, and Subra Suresh. 2015. “Kinetics of Sickle Cell Biorheology and Implications for Painful Vasoocclusive Crisis.” *Proceedings of the National Academy of Sciences of the United States of America* 112 (5): 1422–27. doi:10.1073/pnas.1424111112.

Eddington, David T. 2006. “In-Line Microfluidic Bubble Trap.” *Chips and Tips*. http://blogs.rsc.org/chipsandtips/2006/11/22/in-line-microfluidic-bubble-trap/.

El-Ali, Jamil, Suzanne Gaudet, Axel Günther, Peter K. Sorger, and Klavs F. Jensen. 2005. “Cell Stimulus and Lysis in a Microfluidic Device with Segmented Gas−Liquid Flow.” *Analytical Chemistry* 77 (11): 3629–36. doi:10.1021/ac050008x.

Garstecki, Piotr, Michael J Fuerstman, Michael A. Fischbach, Samuel K. Sia, and George M. Whitesides. 2006. “Mixing with Bubbles: A Practical Technology for Use with Portable Microfluidic Devices.” *Lab on a Chip* 6 (2): 207–12. doi:10.1039/b510843h.

Günther, Axel, Manish Jhunjhunwala, Martina Thalmann, Martin A. Schmidt, and Klavs F. Jensen. 2005. “Micromixing of Miscible Liquids in Segmented Gas−Liquid Flow.” *Langmuir* 21 (4): 1547–55. doi:10.1021/la0482406.

Hettiarachchi, Kanaka, and Abraham Lee. 2008. “Venturi-Based Two-Layer Microfluidic Pumping System.” In . San Diego, California, USA.

Higgins, J. M., D. T. Eddington, S. N. Bhatia, and L. Mahadevan. 2007. “Sickle Cell Vasoocclusion and Rescue in a Microfluidic Device.” *Proceedings of the National Academy of Sciences* 104 (51): 20496–500. doi:10.1073/pnas.0707122105.

Jackel, J. L., J. J. Johnson, and W. J. Tomlinson. 1990. “Bistable Optical Switching Using Electrochemically Generated Bubbles.” *Optics Letters* 15 (24): 1470–72.

Jensen, Mads Jakob, Goran Goranović, and Henrik Bruus. 2004. “The Clogging Pressure of Bubbles in Hydrophilic Microchannel Contractions.” *Journal of Micromechanics and Microengineering* 14 (7): 876. doi:10.1088/0960-1317/14/7/006.

Johnson, M., G. Liddiard, M. Eddings, and B. Gale. 2008. “Bubble Inclusion and Removal Using PDMS Membrane-Based Gas Permeation for Applications in Pumping and Mixing in Microfluidic Devices.” In , 1006–8.

Johnson, Timothy J., David Ross, and Laurie E. Locascio. 2002. “Rapid Microfluidic Mixing.” *Analytical Chemistry* 74 (1): 45–51.

Kang, Edward, Dae Ho Lee, Chang-Beom Kim, Sung Ju Yoo, and Sang-Hoon Lee. 2010. “A Hemispherical Microfluidic Channel for the Trapping and Passive Dissipation of Microbubbles.” *Journal of Micromechanics and Microengineering* 20 (4): 045009. doi:10.1088/0960-1317/20/4/045009.

Kang, Joo H., Yu Chang Kim, and Je-Kyun Park. 2008. “Analysis of Pressure-Driven Air Bubble Elimination in a Microfluidic Device.” *Lab on a Chip* 8 (1): 176–78. doi:10.1039/b712672g.

Kao, Jonathan, Xiaolin Wang, John Warren, Jie Xu, and Daniel Attinger. 2007. “A Bubble-Powered Micro-Rotor: Conception, Manufacturing, Assembly, and Characterization.” *Journal of Micromechanics and Microengineering* 17 (12): 2454–60. doi:10.1088/0960-1317/17/12/010.

Karlsson, J. Mikael, Muriel Gazin, Sanna Laakso, Tommy Haraldsson, Surbhi Malhotra-Kumar, Minna Mäki, Herman Goossens, and Wouter van der Wijngaart. 2013. “Active Liquid Degassing in Microfluidic Systems.” *Lab on a Chip* 13 (22): 4366–73. doi:10.1039/c3lc50778e.

Kohnle, J., G. Waibel, R. Cernosa, M. Storz, H. Ernst, H. Sandmaier, T. Strobelt, and R. Zengerle. 2002. “A Unique Solution for Preventing Clogging of Flow Channels by Gas Bubbles.” In *The Fifteenth IEEE International Conference on Micro Electro Mechanical Systems, 2002*, 77–80. doi:10.1109/MEMSYS.2002.984094.

Kolnik, Martin, Lev S. Tsimring, and Jeff Hasty. 2012. “Vacuum-Assisted Cell Loading Enables Shear-Free Mammalian Microfluidic Culture.” *Lab on a Chip* 12 (22): 4732–37. doi:10.1039/C2LC40569E.

Koo, Kyo-in, Sangmin Lee, and Dong-il Dan Cho. 2011. “Fabrication of a Micro-Fluid Gathering Tool for the Gastrointestinal Juice Sampling Function of a Versatile Capsular Endoscope.” *Sensors* 11 (7): 6978–90. doi:10.3390/s110706978.

Kreutzer, Michiel T., Freek Kapteijn, Jacob A. Moulijn, and Johan J. Heiszwolf. 2005. “Multiphase Monolith Reactors: Chemical Reaction Engineering of Segmented Flow in Microchannels.” *Chemical Engineering Science*, 7th International Conference on Gas-Liquid and Gas-Liquid-Solid Reactor Engineering, 60 (22): 5895–5916. doi:10.1016/j.ces.2005.03.022.

Krevelen, D. W. van, and Klaas te Nijenhuis. 2009. *Properties of Polymers: Their Correlation with Chemical Structure; Their Numerical Estimation and Prediction from Additive Group Contributions*. Elsevier.

Liang, David Y., Augusto M. Tentori, Ivan K. Dimov, and Luke P. Lee. 2011. “Systematic Characterization of Degas-Driven Flow for Poly(dimethylsiloxane) Microfluidic Devices.” *Biomicrofluidics* 5 (2). doi:10.1063/1.3584003.

Liu, Changchun, Jason A. Thompson, and Haim H. Bau. 2011. “A Membrane-Based, High-Efficiency, Microfluidic Debubbler.” *Lab on a Chip* 11 (9): 1688–93. doi:10.1039/c1lc20089e.

Liu, R. H., M. A. Stremler, K. V. Sharp, M. G. Olsen, J. G. Santiago, R. J. Adrian, H. Aref, and D. J. Beebe. 2000. “Passive Mixing in a Three-Dimensional Serpentine Microchannel.” *Journal of Microelectromechanical Systems* 9 (2): 190–97. doi:10.1109/84.846699.

Locascio, L. E., C. E. Perso, and C. S. Lee. 1999. “Measurement of Electroosmotic Flow in Plastic Imprinted Microfluid Devices and the Effect of Protein Adsorption on Flow Rate.” *Journal of Chromatography. A* 857 (1-2): 275–84.

Lochovsky, Conrad, Sanjesh Yasotharan, and Axel Günther. 2012. “Bubbles No More: In-Plane Trapping and Removal of Bubbles in Microfluidic Devices.” *Lab on a Chip* 12 (3): 595–601. doi:10.1039/C1LC20817A.

Lötters, J C, W Olthuis, P H Veltink, and P Bergveld. 1997. “The Mechanical Properties of the Rubber Elastic Polymer Polydimethylsiloxane for Sensor Applications.” *Journal of Micromechanics and Microengineering* 7 (3): 145–47. doi:10.1088/0960-1317/7/3/017.

Luo, Chunxiong, Xuejun Zhu, Tao Yu, Xianjia Luo, Qi Ouyang, Hang Ji, and Yong Chen. 2008. “A Fast Cell Loading and High-Throughput Microfluidic System for Long-Term Cell Culture in Zero-Flow Environments.” *Biotechnology and Bioengineering* 101 (1): 190–95. doi:10.1002/bit.21877.

Macounová, Kateřina, Catherine R. Cabrera, Mark R. Holl, and Paul Yager. 2000. “Generation of Natural pH Gradients in Microfluidic Channels for Use in Isoelectric Focusing.” *Analytical Chemistry* 72 (16): 3745–51. doi:10.1021/ac000237d.

Meng, Dennis Desheng, Joonwon Kim, and Chang-Jin Kim. 2006. “A Degassing Plate with Hydrophobic Bubble Capture and Distributed Venting for Microfluidic Devices.” *Journal of Micromechanics and Microengineering* 16 (February): 419–24. doi:10.1088/0960-1317/16/2/028.

Monahan, Jennifer, Andrew A. Gewirth, and Ralph G. Nuzzo. 2001. “A Method for Filling Complex Polymeric Microfluidic Devices and Arrays.” *Analytical Chemistry* 73 (13): 3193–97. doi:10.1021/ac001426z.

Ng, Jessamine M. K., Irina Gitlin, Abraham D. Stroock, and George M. Whitesides. 2002. "Components for Integrated Poly(dimethylsiloxane) Microfluidic Systems." *Electrophoresis* 23 (20): 3461–73. doi:10.1002/1522-2683(200210)23:20<3461::AID-ELPS3461>3.0.CO;2-8.

Nguyen, Nam-Trung, and Steven T. Wereley. 2006. *Fundamentals and Applications of Microfluidics*. Second. Artech House.

Olsen, Kimberly G., David J. Ross, and Michael J. Tarlov. 2002. "Immobilization of DNA Hydrogel Plugs in Microfluidic Channels." *Analytical Chemistry* 74 (6): 1436–41.

Panigrahi, Pradipta Kumar. 2015. *Transport Phenomena in Microfluidic Systems*. John Wiley & Sons.

Perdigones, F., A. Luque, and J. M. Quero. 2010. "PDMS Microdevice for Precise Liquid Aspiration in the Submicroliter Range Based on the Venturi Effect." *Microelectronic Engineering* 87 (11): 2103–9. doi:10.1016/j.mee.2010.01.006.

Selva, Bertrand, Vincent Miralles, Isabelle Cantat, and Marie-Caroline Jullien. 2010. "Thermocapillary Actuation by Optimized Resistor Pattern: Bubbles and Droplets Displacing, Switching and Trapping." *Lab on a Chip* 10 (14): 1835–40. doi:10.1039/c001900c.

Skelley, Alison M., and Joel Voldman. 2008. "An Active Bubble Trap and Debubbler for Microfluidic Systems." *Lab on a Chip* 8 (10): 1733–37. doi:10.1039/b807037g.

Stroock, Abraham D., Stephan K. W. Dertinger, Armand Ajdari, Igor Mezić, Howard A. Stone, and George M. Whitesides. 2002. "Chaotic Mixer for Microchannels." *Science* 295 (5555): 647–51. doi:10.1126/science.1066238.

Sung, Jong Hwan, and Michael L. Shuler. 2009. "Prevention of Air Bubble Formation in a Microfluidic Perfusion Cell Culture System Using a Microscale Bubble Trap." *Biomedical Microdevices* 11 (4): 731–38. doi:10.1007/s10544-009-9286-8.

Trung, Nguyen Ba, Masato Saito, Haruo Takabayashi, Pham Hung Viet, Eiichi Tamiya, and Yuzuru Takamura. 2010. "Multi-Chamber PCR Chip with Simple Liquid Introduction Utilizing the Gas Permeability of Polydimethylsiloxane." *Sensors and Actuators B: Chemical* 149 (1): 284–90. doi:10.1016/j.snb.2010.06.013.

van Lintel, Harald, Guillaume Mernier, and Philippe Renaud. 2012. "High-Throughput Micro-Debubblers for Bubble Removal with Sub-Microliter Dead Volume." *Micromachines* 3 (2): 218–24. doi:10.3390/mi3020218.

Wang, Joseph, Martin Pumera, Madhu Prakash Chatrathi, Alberto Escarpa, Renate Konrad, Anja Griebel, Wolfgang Dörner, and Holger Löwe. 2002. “Towards Disposable Lab-on-a-Chip: Poly(methylmethacrylate) Microchip Electrophoresis Device with Electrochemical Detection.” *Electrophoresis* 23 (4): 596–601. doi:10.1002/1522-2683(200202)23:4<596::AID-ELPS596>3.0.CO;2-C.

Wang, Yong, Dongyoung Lee, Lisa Zhang, Hyojin Jeon, Joshua E. Mendoza-Elias, Tricia A. Harvat, Sarah Z. Hassan, Amanda Zhou, David T. Eddington, and José Oberholzer. 2012. “Systematic Prevention of Bubble Formation and Accumulation for Long-Term Culture of Pancreatic Islet Cells in Microfluidic Device.” *Biomedical Microdevices* 14 (2): 419–26. doi:10.1007/s10544-011-9618-3.

Weigl, Bernhard H., Jennah Kriebel, Kelly J. Mayes, Todd Bui, and Paul Yager. 1999. “Whole Blood Diagnostics in Standard Gravity and Microgravity by Use of Microfluidic Structures (T-Sensors).” *Microchimica Acta* 131 (1-2): 75–83. doi:10.1007/s006040050011.

Whitesides, George M. 2006. “The Origins and the Future of Microfluidics.” *Nature* 442 (7101): 368–73. doi:10.1038/nature05058.

Whitesides, G. M., E. Ostuni, S. Takayama, X. Jiang, and D. E. Ingber. 2001. “Soft Lithography in Biology and Biochemistry.” *Annual Review of Biomedical Engineering* 3: 335–73. doi:10.1146/annurev.bioeng.3.1.335.

Xia, Younan, and George M. Whitesides. 1998. “Soft Lithography.” *Angewandte Chemie International Edition* 37 (5): 550–75. doi:10.1002/(SICI)1521-3773(19980316)37:5<550::AID-ANIE550>3.0.CO;2-G.

Xu, Jie, Regis Vaillant, and Daniel Attinger. 2010. “Use of a Porous Membrane for Gas Bubble Removal in Microfluidic Channels: Physical Mechanisms and Design Criteria.” *Microfluidics and Nanofluidics* 9 (4-5): 765–72. doi:10.1007/s10404-010-0592-5.

Yang, Zhen, Sohei Matsumoto, and Ryutaro Maeda. 2002. “A Prototype of Ultrasonic Micro-Degassing Device for Portable Dialysis System.” *Sensors and Actuators A: Physical*, Papers from the Proceedings of the 14th IEEE Internat. Conf. on MicroElectroMechanical Systems, 95 (2–3): 274–80. doi:10.1016/S0924-4247(01)00741-5.

Yu, H., D. Li, R. C. Roberts, K. Xu, and N. C. Tien. 2012. “Design, Fabrication and Testing of a Micro-Venturi Tube for Fluid Manipulation in a Microfluidic System.” *Journal of Micromechanics and Microengineering* 22 (3): 035010. doi:10.1088/0960-1317/22/3/035010.

Zheng, Wenfu, Zhuo Wang, Wei Zhang, and Xingyu Jiang. 2010. “A Simple PDMS-Based Microfluidic Channel Design That Removes Bubbles for Long-Term on-Chip Culture of Mammalian Cells.” *Lab on a Chip* 10 (21): 2906–10. doi:10.1039/c005274d.

Zhou, Xuechang, Lana Lau, Wendy Wai Ling Lam, Shannon Wing Ngor Au, and Bo Zheng. 2007. "Nanoliter Dispensing Method by Degassed Poly(dimethylsiloxane) Microchannels and Its Application in Protein Crystallization." *Analytical Chemistry* 79 (13): 4924–30. doi:10.1021/ac070306p.

Zhu, Xiaoshan. 2009. "Micro/nanoporous Membrane Based Gas–water Separation in Microchannel." *Microsystem Technologies* 15 (9): 1459–65. doi:10.1007/s00542-009-0903-5.

## APPENDIX

```
%% Bubble Volume Removal Code
%This is code is used to measure the volume of a single bubble surrounded by
two high fluorescent intensities
%Created by Theodore Christoforidis
%Modified by Carlos Ng

Clc
clear all
close all

tic
cd '/Users/carlosfng/Desktop/90_microns' %%Find the folder with images.
files=dir;
str = {files.name};
[selected,cancel] = listdlg('PromptString','Select a file:', 'ListSize', [600
450],...'SelectionMode','multiple', 'ListString',str);

LENGTH=[];
   for IndexSelected=1:length(selected) %% Select all figures
   ExpNo=selected(IndexSelected);      %% Number of all Figures plus 2 Spaces
   name=files(ExpNo).name ;
   Incidence1=0;

     if IndexSelected==1
        figure(1)
        title('first picture original')
        I = imread(name);
        imagesc(I);
        impixelinfo
prompt = {'Enter Yleft','Enter Yright'}; %Ask user the channel that wants to
be measured
        dlg_title = 'Input';
        num_lines = 1;
        def = {'1','2'};
        answer = inputdlg(prompt,dlg_title,num_lines,def);
        XL=str2double(answer(1));%%% Number of different experiments %%%
        XR=str2double(answer(2));
      end

 double(I)
 I = imread(name);      %% Image in numbers
 [X,Y]=size(I);         %% size of the matrix

%%%%% THIS part leaves all the dark parts and THE REST all get SUPER BRIGHT
for ii=1:Y
    for jj=1:X
     if I(jj,ii)>20000
     I(jj,ii)=500000;
     end
    end
end
for ii=XL:XR
    Incidence1=0;
for jj=8:Y-8 %%(columns - 8)
     if I(ii,jj-7)>20000
```

```
      if  I(ii,jj-1)>20000
       if I(ii,jj)<20000
        if Incidence1==0
           Incidence1=Incidence1+1;
           Start=jj;
        end
       end
      end
     end
     %end
    if Incidence1==1
     if I(ii,jj+7)>20000
      if  I(ii,jj+1)>20000
       if I(ii,jj)<20000
          End=jj;
       end
      end
     end
    end
  end
   LENGTH=[LENGTH ; IndexSelected End-Start];
 end
end

figure(2)
imagesc(I);
impixelinfo

figure(3)
plot(LENGTH(:,1),LENGTH(:,2))
xlabel('Time(seconds)');
ylabel('Fluorescence(Pixels)');

%%%CLEAN
figure(4)
T=sprintf('From position %d to %d',XL,XR)
title(T)
plot(LENGTH(:,1),LENGTH(:,2),'x')
xlabel('Time(seconds)');
ylabel('Fluorescence(Pixels)');
Calibration=(1/0.650); %Calibration (0.650 pixels/microns)
Volumeincubicmicrons = Calibration*LENGTH(:,2)*12*15; % Volume Calculation
(Height*Width*length) Height= 12 microns, Width= 15 microns
Volumeinpicoliter = Volumeincubicmicrons*(1/1000) %%(1 pL = 1000 um3)
time = (1:1:numel(Volumeinpicoliter))'; %Time it took the bubble to disappear

figure (5)
plot(time,Volumeinpicoliter)
xlabel('Time(seconds)');
ylabel('Volume(picoliters)');
hold on
% toc
```

# VITA

## Carlos F. Ng Pitti

**Education**

**University of Illinois at Chicago (UIC)** **Expected Graduation: May 2016**
Master of Science in Bioengineering
Advisor: David Eddington

**University of Illinois at Chicago (UIC)** **May 2012**
Bachelor of Science in Bioengineering
Graduated Cum Laude

**Experience**

**Biological Microsystems Laboratory,** Chicago, IL **Sept 2014-Present**
Graduate Research Assistant

- Develop an air bubble extraction tool for microfluidic devices
- Quantify the bubble extraction rate
- Extraction of bubbles using different channel designs
- Design a microfluidic device for the study of vasooclusion

**Chicago Microenvironmental Control Foundry,** Chicago, IL **Sept 2012-Aug 2014**
Microfabrication Engineer

- Design microfluidic devices and micropattern templates
- Enhance microfluidic devices provided by collaborators
- Contribute to the distribution of microfluidic tools to local researchers

**Biological Microsystems Laboratory,** Chicago, IL **Jan 2012-Aug 2012**
Research Assistant

- Fabricate micro-devices for capture of tumor cells
- Able to perform cell culture of certain types of cancer cells
- Competent of microscopic image analysis

**INDICASAT-AIP,** Panama City, Panama **Summer Internship 2011**
Neuroscientist Assistant

- Established a protocol for analyzing neurophysiological data
- Dominate a specialized data acquisition system and software
- Contribute in the development of a neural recording procedure

**Skills**

Extensive technical writing and scientific presentation experience.
Experience in training new staff
Technical expertise in photolithography and soft lithography
Knowledge on Microsoft Office, MetaMorph, ImageJ, AutoCAD, SolidWorks and Matlab
Foreign Language: Fluent in Spanish

**Awards**

Abraham Lincoln Fellowship 2014-2015
Supporting Excellence Endowment 2011-2012
Thomas A. Bullen Scholarship 2009